Clouds as Seen by Satellite Sounders (3I) and Imagers (ISCCP). Part I: Evaluation of Cloud Parameters

C. J. STUBENRAUCH

Laboratoire de Météorologie Dynamique du CNRS, Ecole Polytechnique, Palaiseau, France

W. B. ROSSOW

NASA/Goddard Space Flight Center, Institute for Space Studies, New York, New York

F. CHÉRUY, A. CHÉDIN, AND N. A. SCOTT

Laboratoire de Météorologie Dynamique du CNRS, Ecole Polytechnique, Palaiseau, France

(Manuscript received 28 October 1997, in final form 1 April 1998)

ABSTRACT

The improved initialization inversion (3I) algorithms convert TIROS-N Operational Vertical Sounder observations from the National Oceanic and Atmospheric Administration (NOAA) polar-orbiting environmental satellites into atmospheric temperature and water vapor profiles, together with cloud and surface properties. Their relatively good spectral resolution and coverage make IR sounders a very useful tool for the determination of cloud properties both day and night. The iterative process of detailed comparisons between cloud parameters obtained from this global dataset, which is available in the framework of the NOAA–National Aeronautics and Space Administration Pathfinder Program, with time–space-collocated observations of clouds from the recently reprocessed International Satellite Cloud Climatology Project (ISCCP) dataset has led to an improved 3I cloud analysis scheme based on a weighted-χ^2 method described in the second article of this series. This process also provides a first evaluation of the ISCCP reanalysis. The new 3I cloud scheme obtains cloud properties very similar to those from ISCCP for homogeneous cloud scenes. Improvement is especially notable in the stratocumulus regimes where the new 3I scheme detects much more of the low-level cloudiness. Remaining discrepancies in cloud classification can now be explained by differences in cloud detection sensitivity, differences in temperature profiles used, and inhomogeneous or partly cloudy fields. Cirrus cloud identification during the daytime in the recent ISCCP dataset is improved relative to the first version of ISCCP, but is still an underestimate. At night only multispectral IR analyses like 3I can provide cirrus information. The reprocessed ISCCP dataset also shows considerable improvement in cloud cover at higher latitudes. Differences in 3I and ISCCP summertime cloud cover over deserts may be caused by different sensitivities to dust storms.

1. Introduction

Clouds play a key role in Earth's radiation balance, so it is important to gather as much reliable information on their properties and global distributions as is available in order to gain a better understanding of their interaction with the surrounding atmosphere. For climate studies, observations from space have an advantage of global coverage with high space–time resolution. However, complex retrieval algorithms are necessary to convert satellite-measured radiances, which have been backscattered or emitted by the atmosphere or clouds, into atmospheric, cloud, and surface properties.

The most extensive global cloud climatology is the one being produced by the International Satellite Cloud Climatology Project (ISCCP, Rossow and Schiffer 1991). ISCCP provides cloud information three-hourly with a relatively good spatial resolution (about 30 km) using one visible (day only) and one atmospheric window IR (day and night) channel from imagers onboard geostationary and polar-orbiting weather satellites. Radiances are converted into cloud parameters with the help of a radiative transfer model and auxiliary data like atmospheric temperature profiles from the operational TIROS-N Operational Verticle Sounder (TOVS) system. This ISCCP dataset has been thoroughly studied (e.g., Fu et al. 1990; Tselioudis et al. 1992; Klein and Hartmann 1993; Machado and Rossow 1993; Cairns 1995; Liao et al. 1995; Lau and Crane 1995). Some of these

Corresponding author address: Dr. Claudia Stubenrauch, Laboratoire de Météorologie Dynamique du C.N.R.S., Ecole Polytechnique, 91128 Paliseau Cedex, France.
E-mail: stubenrauch@lmdx.polytechnique.fr

studies have led to a recent reanalysis (Rossow et al. 1996), mostly improving the treatment of cirrus and polar clouds, as will be shown in the following.

Another important source of cloud information (day and night) can be found in measurements from IR sounders. Their coarse spatial resolution (20–100 km) should have less effect on determining the properties of clouds with larger spatial extents like cirrus. Cloud climatologies are being produced from these instruments on polar-orbiting satellites by Wylie and Menzel (1999), Susskind et al. (1997), and Chédin et al. (1997).

Before undertaking climate studies, it is important to evaluate the quality of these cloud products. The subject of the following articles is the evaluation of the cloud parameters obtained with the improved initialization inversion (3I) method on a global scale by comparison with time–space collocated ISCCP clouds, which are being intensively checked by many ongoing studies. Since during this study process the ISCCP algorithms have undergone considerable change (Rossow et al. 1996), we also used the recently reprocessed ISCCP dataset to evaluate its improvement.

Our results are reported in three articles. The first (this paper) describes the iterative comparison process between two versions of the 3I and two versions of the ISCCP cloud parameters. This comparison study led to the development of a new 3I cloud scheme that is described in the second article (Stubenrauch et al. 1999a, henceforth paper 2). A third article (Stubenrauch et al. 1998b, henceforth paper 3) investigates further the correlations between 3I and ISCCP cloud parameters under different conditions of spatial heterogeneity and studies cloud radiative effects on the radiation budget in combination with Earth Radiation Budget Experiment (ERBE) flux data.

The methods for obtaining the four different datasets—original and new 3I, original and reprocessed ISCCP—are described in section 2. We then show and interpret comparisons between 3I and ISCCP cloud parameters on a global scale in section 3. After more detailed comparisons of particular cloud types in five different geographical regions in section 4, we summarize our conclusions in section 5.

2. Cloud parameter determination

a. 3I cloud parameters

The 3I algorithm suite (Chédin et al. 1985) determines atmospheric temperature and water vapor profiles, as well as cloud parameters, from High-resolution Infrared Sounder (HIRS)/Microwave Sounding Unit (MSU) observations. It is based on 1) the thermodynamic initial guess retrieval (TIGR) dataset, describing ~2300 different atmospheric conditions extracted from ~180 000 radiosonde measurements (Escobar 1993; Chevallier et al. 1998) and 2) a fast line-by-line radiative transfer model, Automatized Atmospheric Absorption Atlas (4A; Scott and Chédin 1981), simulating clear sky and cloudy radiances at 30 pressure levels.

Cloud detection is performed at HIRS spatial resolution (≈17 km at nadir) by seven (night) or eight (day) threshold tests, relying very much upon comparisons of the simultaneous HIRS and MSU channels, where the latter probe through the clouds. A summary of this cloud detection scheme can be found in Table 2 of Stubenrauch et al. (1996).

Some of the cloud detection tests have been refined in the new 3I scheme. 1) A sea surface temperature (SST) climatology (Shea et al. 1990) now provides the first guess surface temperature used in threshold tests over ocean, replacing a forecast surface temperature used in the local 3I algorithms. 2) Observed visible radiances are now corrected for viewing and illumination geometry dependence as in Derrien et al. (1993). 3) The maximum brightness temperature test is not performed over land areas where topographic height changes by more than 250 m within a 100 km × 100 km box. 4) At polar latitudes, the SST test threshold is set to 7 K instead of 5 K. 5) Seasonal brightness temperature calibration constants were obtained by comparing air-mass-averaged brightness temperatures computed from radiosonde measurements to collocated observed brightness temperatures (Armante et al. 1998). The final cloud detection tests (after including the refinements above) used in the 3I algorithms for the treatment of the National Oceanic and Atmospheric Administration–National Aeronautics and Space Administration Pathfinder TOVS data (Maiden et al. 1994) are summarized in Table 1.

Cloud properties are determined from the average radiance for all cloudy pixels within each 100 km × 100 km box, assuming a single, homogeneous cloud layer. The cloud-top pressure and the effective cloud amount (cloud cover fraction times spectrally averaged emissivity) are obtained as described in sections 2a(1) (original 3I) and 2a(2) (new 3I). More details can be found in paper 2. In the 3I cloud algorithm, the spectrally averaged emissivity over cloudy HIRS pixels is called ''effective cloud amount'' $N\varepsilon_{cld}$, because pixels identified as cloudy can in reality be partly cloudy due to the coarse spatial resolution of the HIRS pixels. The global 3I Pathfinder data have been organized on a 1° lat × 1° long grid. We also determine a cloud cover fraction as the fraction of the total number of pixels in each 1° grid that are cloudy. The effective cloud amount over a 1° grid, henceforth called ''εN,'' is then the product of cloud cover fraction and ''effective cloud amount'' over the cloudy pixels $N\varepsilon_{cld}$. The cloud-top pressure is transformed into cloud-top temperature using the 3I atmospheric temperature profiles.

1) ORIGINAL 3I ''COHERENCE OF EFFECTIVE CLOUD AMOUNT'' METHOD

The original 3I cloud scheme (Wahiche et al. 1986; Stubenrauch et al. 1996) was based on a method that

TABLE 1. The 3I cloud detection scheme at HIRS spatial resolution: if one of these tests is satisfied, the pixel is considered cloudy. Here θ_0 is the solar zenith angle, $f(\theta_0)$ is an angular correction function to the albedo, and ε_{surf} is the microwave surface emissivity. Most of these tests (1, 3, 5, 7, and 9) use surface temperature estimates (T_{surf}) obtained by regressions compared to the TIGR dataset. Test 4 relies on the ability to predict a brightness temperature T measured in one channel by a combination of brightness temperatures from other channels. Again, the regression coefficients a_i and b_i were obtained from comparison to the TIGR dataset.

	Day	Night
1) Frozen sea test		
Sea	$T_{surf}(11\ \mu m) < 271$ K	$T_{surf}(4\ \mu m) < 271$ K
2) Albedo (α) test		
Sea, no polar regions	$\alpha < 15\% + f(\theta_0)$ $\quad f(\theta_0 = 0°) = 0$	
Land	$\alpha > 20\% + f(\theta_0)$ and $T(11\ \mu m) < 285$ K	
3) Window channel tests		
Sea and warm land [$T(11\ \mu m) > 260$ K]	$\lvert T_{surf}(3.7\ \mu m) - T_{surf}(4\ \mu m)\rvert > 12$ K and $\alpha < 20\%$	$T_{surf}(4\ \mu m) - T_{surf}(11\ \mu m) > 2.5$ K or $T_{surf}(4\ \mu m) - T_{surf}(11\ \mu m) < -4$ K or $T_{surf}(3.7\ \mu m) - T_{surf}(4\ \mu m) > 3$ K or $T_{surf}(3.7\ \mu m) - T_{surf}(4\ \mu m) < -4$ K
Sea ice	$T(3.7\ \mu m) - T(4\ \mu m) > 8$ K	$T(4\ \mu m) - T_{surf}(11\ \mu m) > 2$ K or $T(4\ \mu m) - T_{surf}(11\ \mu m) < -1$ K
Cold land [$T(11\ \mu m) < 260$ K]	$T(3.7\ \mu m) - T(4\ \mu m) > 8$ K	$T(4\ \mu m) - T_{surf}(11\ \mu m) > 0.5$ K or $T(4\ \mu m) - T_{surf}(11\ \mu m) < -1.5$ K
4) Interchannel regression tests		
Sea, land, sea ice	$\left\lvert T_7 - \sum_{i=13}^{15} a_i T_i - a_0 \right\rvert > 3.2$ K or $\left\lvert T_{MSU2} - \sum_{i=3}^{7} b_i T_i - b_0 \right\rvert > 2$ K	$\left\lvert T_7 - \sum_{i=13}^{15} a_i T_i - a_0 \right\rvert > 2.7$ K or $\left\lvert T_{MSU2} - \sum_{i=3}^{7} b_i T_i - b_0 \right\rvert > 2$ K
5) Surface temperature test		
Sea	SST(climatology) $- T_{surf}(11\ \mu m) > 5$ K	SST(climatology) $- T_{surf}(4\ \mu m) > 5$ K
Polar sea	SST(climatology) $- T_{surf}(11\ \mu m) > 7$ K	SST(climatology) $- T_{surf}(4\ \mu m) > 7$ K
6) Low cloud test		
Sea, land sea ice		$T(11\ \mu m)$ lns $T(3.7\ \mu m) > 0.5$ K
7) Adjacent spot test		
Sea, no coast	at least 1 neighbor with $T_{surf}(11\ \mu m)^{neigh} - T_{surf}(11\ \mu m) > 1.5$ K or $nb^{neigh} > 2$ and no neighbor with $\lvert T_{surf}(11\ \mu m)^{neigh} - T_{surf}(11\ \mu m)\rvert < 1.5$ K	at least 1 neighbor with $T_{surf}(4\ \mu m)^{neigh} - T_{surf}(4\ \mu m) > 1.5$ K or $nb^{neigh} > 2$ and no neighbor with $\lvert T_{surf}(4\ \mu m)^{neigh} - T_{surf}(4\ \mu m)\rvert < 1.5$ K
Land, altitude difference > 250 m	at least 1 neighbor with $T_{surf}(11\ \mu m)^{neigh} - T_{surf}(11\ \mu m) > 3$ K or $nb^{neigh} > 2$ and no neighbor with $\lvert T_{surf}(11\ \mu m)^{neigh} - T_{surf}(11\ \mu m)\rvert < 3$ K	at least 1 neighbor with $T_{surf}(4\ \mu m)^{neigh} - T_{surf}(4\ \mu m) > 3$ K or $nb^{neigh} > 2$ and no neighbor with $\lvert T_{surf}(4\ \mu m)^{neigh} - T_{surf}(4\ \mu m)\rvert < 3$ K
8) Low cloud over frozen region		
Only polar regions, altitude difference < 250 m	$(T(3.7\ \mu m) - T(11\ \mu m))/\cos\theta_0 > 30°$ and $\varepsilon_{surf} > 0.76$	
9) Maximum temperature test (in box)		
Sea or land, no coast, altitude difference < 250 m	$T_{surf}(11\ \mu m)^{max} - T_{surf}(11\ \mu m) > 4$ K	$T_{surf}(11\ \mu m)^{max} - T_{surf}(11\ \mu m) > 4$ K

assumes that the effective cloud amount is ''coherent'' (should have similar values) among the four HIRS spectral channels (numbers 4–7) in the 15-μm CO_2 band (with peak signal arising from levels between 400 and 900 hPa) and the 11-μm IR window channel (number 8). The effective cloud amount over cloudy HIRS pixels, $N\varepsilon_{cld}$, was calculated at various cloud pressure levels, k, and for each channel, i, as:

$$N\varepsilon(p_k, \nu_i) = \frac{I_m(\nu_i, \theta) - I_{clr}(\nu_i, \theta)}{I_{cld}(p_k, \nu_i, \theta) - I_{clr}(\nu_i, \theta)}, \qquad (1)$$

with cloud pressure levels $k = 1, 30$ and channel numbers $i = 4, \ldots, 8$; measured radiance I_m; retrieved clear sky radiance I_{clr}; and calculated radiance I_{cld} emitted by a homogeneous opaque single cloud layer, at the corresponding viewing zenith angle θ.

Before calculating the relative dispersion of the effective cloud amount within the spectral interval of the five HIRS channels, $\sigma[N\varepsilon(p_k, \nu_i)]/\overline{N\varepsilon(p_k)}$, at each pressure level k, noisy channels i, with $|N\varepsilon(p_k, \nu_i) - \overline{N\varepsilon(p_k)}| > 0.2$, were first eliminated (testing in the following order: channel number 4, 5, 7, 8 and then 6). This means that only channels with an effective cloud amount within 0.2 from the frequency averaged effective cloud amount were used in the calculation at a specific pressure level k. The pressure level was eliminated if only one channel is left. Finally, the cloud-top was assigned to the pressure level that gives the minimum relative dispersion $\sigma[N\varepsilon(p_k, \nu_i)]/\overline{N\varepsilon(p_k)}$ of the effective cloud amount within the spectral interval of the remaining HIRS channels.

In the calculation procedure no further cuts were made on the values of $N\varepsilon(p_k, \nu_i)$ or $\overline{N\varepsilon(p_k)}$ (especially $N\varepsilon \in [0, 1]$). However, negative values of $N\varepsilon(p_k, \nu_i)$, which can occur in the case of low clouds when the method becomes unstable (denominator approaching zero), were set to 1.2 if $I_m/I_{cld} \leq 1$ or else to 0, based on a simulation with the general circulation model (GCM) of the Goddard Institute for Space Studies (GISS). Also, if $\overline{N\varepsilon(p_k)}$ exceeds 1.5, it was set to this value for finding the pressure level with the minimum relative dispersion.

2) NEW 3I χ^2_w METHOD

As the comparison of original 3I and ISCCP results will show, the 3I cloud parameter extraction method needed another revision to reduce the biases for low-level clouds, especially in the marine stratocumulus regimes. A weighted-χ^2 method has been developed, based on calculating the mean effective cloud amount at all pressure levels over all CO_2-band channels, using spectral channel- and cloud-level dependent weights. The principle is quite simple: by minimizing χ^2_w in Eq. (2), which is equivalent to $d\chi^2_w/dN\varepsilon(p_k) = 0$, one obtains the effective cloud amount and the corresponding cloud-top pressure:

$$\chi^2_w(p_k) = \sum_{i=4}^{8} \left\langle \frac{\{[I_{cld}(p_k, \nu_i) - I_{clr}(\nu_i)]N\varepsilon(p_k) - [I_m(\nu_i) - I_{clr}(\nu_i)]\}^2}{\sigma^2(\nu_i)} \right\rangle W^2(p_k, \nu_i), \qquad (2)$$

$\sigma(\nu_i)$ corresponds to the instrument noise, which is supposed to be channel independent like in Eyre and Menzel (1989).

The empirical weights $W^2(p_k, \nu_i)$, depending on cloud-level k and frequency ν_i, have been developed to take account the effect of the temperature profile uncertainty on the radiance difference $I_{clr}(\nu_i) - I_{cld}(p_k, \nu_i)$. The method and the determination of the empirical weights are described in detail in paper 2.

Essentially, the 3I cloud method assumes that the presence of a cloud in the 100-km region produces a spatially coherent effect on the observed radiances (cf. Coackley and Bretherton 1982), even if the magnitude of this effect is smaller than the channel noise for individual pixels.

b. ISCCP cloud parameters

The first ISCCP dataset (C-series of cloud products; Rossow and Schiffer 1991) has been extensively compared with various other datasets (e.g., Rossow et al. 1993; Lin and Rossow 1994; Liao et al. 1995; Jin et al. 1996). Recently, the ISCCP data have been reprocessed (D-series of cloud products; Rossow et al. 1996). The most important changes made are the use: 1) of the Advanced Very High Resolution Radiometer (AVHRR) 3.7-μm channel for cloud detection over snow and ice surfaces at latitudes higher than 50°, 2) of a lower IR threshold for cloud detection over land, and 3) of an ice crystal model for cloud optical thickness (Mishchenko et al. 1996) and top temperature for cold-topped clouds, leading to smaller optical thicknesses and lower top temperatures for ice clouds.

To obtain global coverage with good time sampling (three hourly), ISCCP collects IR (day and night) and VIS (day only) radiance measurements from both geostationary satellites (covering latitudes from −50° to 50°) and polar orbiters. ISCCP pixel-level data (first version = CX, reprocessed version = DX) have a spatial resolution of about 5 km, sampled every 30 km, which

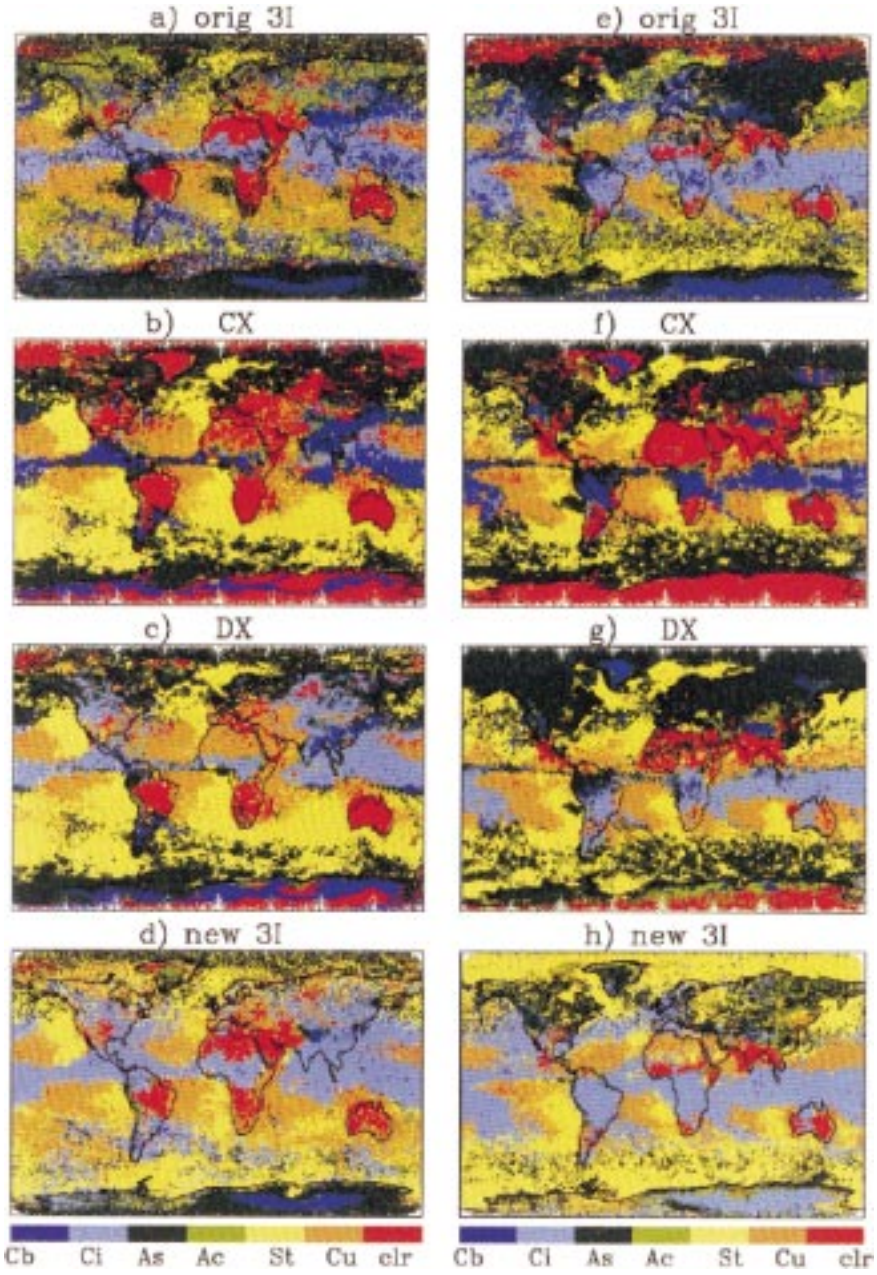

FIG. 1. Geographical maps of the most frequent cloud type at 0730 LT in Jul 1987 [(a)–(d) daylight on Northern Hemisphere] and in Jan 1988 [(e)–(h) daylight on Southern Hemisphere] with cloud types identified by (a), (e) original 3I; (b), (f) current ISCCP (CX); (c), (g) reprocessed ISCCP (DX); and (d), (h) new 3I.

means that about one pixel out of 36 is kept but the statistics of cloud variations are preserved (Sèze and Rossow 1991). Cloud cover fraction for an area is estimated by counting the fraction of all pixels that are determined to be cloudy.

Clouds are detected by IR and VIS threshold tests (plus 3.7-μm tests at higher latitudes) that compare the measured radiances to clear sky composite radiances, which have been estimated from pixels exhibiting low spatial and temporal variability (Rossow and Garder 1993a). In the IR, these reference clear sky radiances come from the locally warmest pixels at each time (within 6.5 K over land and 3.5 K over ocean) within an area of about 100 km $\times$ 100 km over land and of about 450 km $\times$ 450 km (Tropics) to 270 km lat $\times$ 750 km long (midlatitudes) over ocean, which have similar temperatures (within 2.5 K over land and 1.1 K over ocean) compared to values at the same location on the previous

TABLE 2. Definition of six cloud types according to three cloud-top pressure intervals and two intervals of opacity. Opacity is distinguished by ISCCP through cloud optical thickness τ alone (for high clouds) or through optical thickness τ and cloud cover cov (for midlevel and low-level clouds) and by 3I through effective cloud amount of cloudy pixels, $N\varepsilon_{cld}$, (for high clouds) and effective cloud amount over the whole 1° grid, εN (for midlevel and low-level clouds).

ISCCP: τ		< 9.4
3I: $N\varepsilon_{cld}$		< 0.9
P_{cld}	*h*igh opaque: Cb	Cirrus: Ci
440 hPa		
	Altostratus: As	Altocumulus: Ac
680 hPa		
	Stratus: St	Cumulus: Cu
3I: εN	>0.5	
ISCCP:	$\tau > 9.4 \wedge$ cov > 0.5	

and the following day at the same time each day. Clear sky statistics are collected over 5 days (short-term statistics) and 15 days (long-term statistics) over land and over 15 days and 30 days, respectively, over ocean.

For cloudy pixels, cloud-top temperature (and pressure) and optical thickness τ (only during day) are retrieved, assuming a single, homogeneous cloud layer covers each pixel (a region of about 5 km × 5 km). Based on these cloud properties, each cloudy pixel can be classified into one of nine cloud types (only during day), according to three cloud-top pressure intervals and three optical thickness intervals. At night, only cloud-top temperature (pressure) is determined from the IR radiance assuming all clouds are opaque. During daytime, τ is determined from the visible reflectance. In the C-series results for all clouds and in the D-series for clouds with top temperatures >260 K, the τ retrieval assumes that the cloud is composed of spherical liquid droplets with a gamma size distribution defined by an effective radius of 10 μm and effective variance of 0.15. In the D-series results only, the τ retrieval for clouds with top temperatures <260 K assumes that the clouds are composed of fractal ice crystals with a −2 power-law size distribution between 20 and 50 μm that has an effective size of 30 μm and an effective variance of 0.1. If the cloud is not opaque ($\tau_{IR} < 5.5$), the cloud-top temperature is corrected for transmitted radiation as a function of optical thickness.

In the ISCCP results, cloud-top temperatures are converted to cloud-top pressures using the atmospheric temperature profiles produced at 2.5° spatial resolution from the operational TOVS system (McMillin and Dean 1982; Kidwell 1995). Only one profile per day is available. The original TOVS atmospheric temperature layers between 1000, 850, 700, 500, 400, 300, 200, 100, 70, 50, and 30 hPa have been converted to temperatures of the seven ISCCP standard atmospheric layers between 1000, 800, 680, 560, 440, 310, 180, and 30 hPa by linear interpolation in pressure coordinates. The surface and tropopause pressures modify the actual extent of the lower and higher layers in the troposphere.

c. Combined ISCCP–3I data

The 3I cloud parameters (from *NOAA-10* HIRS/MSU) and ISCCP (from *NOAA-10* AVHRR) pixel data (observations at ~0730 local time) have been combined into 1° lat × 1° long grid boxes for July 1987 and January 1988. AVHRR measurements are distributed in the global area coverage (GAC) format, the initial spatial resolution of 1 km deteriorated to about 1 km × 4 km by averaging four pixels in a line and sampling every fifth line. Differences between the AVHRR-based ISCCP results and those from geostationary satellites are generally less than a few percent (Rossow and Garder 1993b; Rossow and Cairns 1995). The data have been divided into morning (am) and evening (pm) observations. Starting from the pixel-level observations allows for a simultaneous, collocated comparison and combined use of the different cloud information. The ISCCP dataset can be used for the validation of the 3I cloud parameters only during daylight conditions when both the VIS and IR radiance information is available. For this particular orbit and these 2 months, daytime data are available only in the summer hemisphere. If during daytime the 3I cloud parameters are reliable, then they can be used to give equally reliable information during nighttime, since the 3I method exploits the IR domain.

3. Global comparisons

a. Geographical maps of most frequent cloud types

To get a first impression of the distribution of cloud properties over the globe, we show a map of the most frequent cloud types in July 1987 and in January 1988 obtained from original 3I cloud scheme (Figs. 1a,e), the first ISCCP results (Figs. 1b,f), the reprocessed ISCCP results (Figs. 1c,g), and from the new 3I cloud scheme (Figs. 1d,h). Henceforth, these results will be referred to as orig-3I, ISCCP CX, ISCCP DX, and new-3I results. For clarity, we consider only six cloud types distinguished by cloud-top pressure in three intervals (midlevel clouds have tops between 680 hPa and 440 hPa) and two effective cloud amounts. Cirrus clouds are separated from high opaque clouds by $N\varepsilon_{cld} = 0.90$ and all other clouds are divided by $\varepsilon N = 0.50$. These cloud types with their properties are summarized in Table 2.

The ISCCP analysis determines optical thickness for each cloudy pixel and can be used to estimate cloud cover from the number of cloudy pixels within the 1° × 1° grid. To approximate the 3I cloud types with the ISCCP results, we explore two alternative schemes. In the first scheme, the cloud-top pressure category is determined by the most frequent value of cloud-top pressure within the 1° grid, whereas in the second scheme,

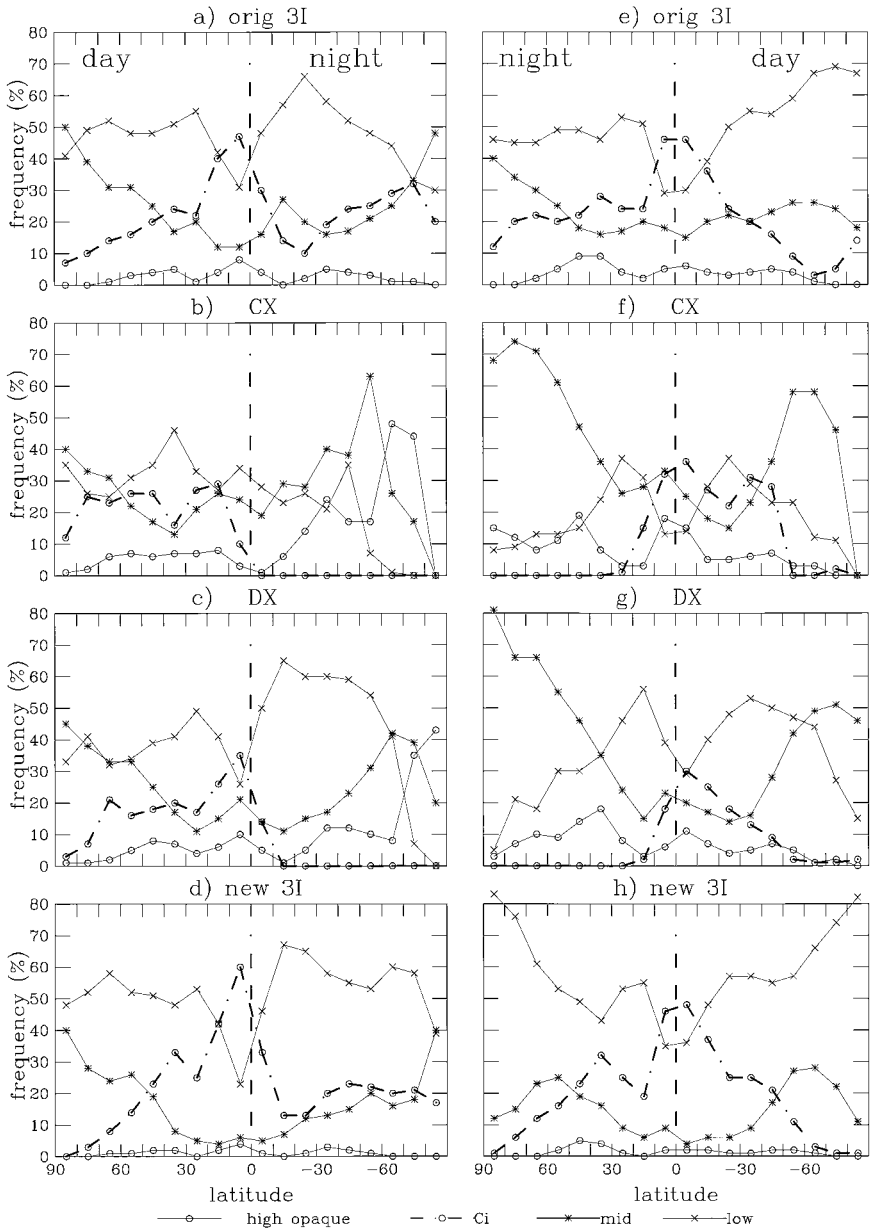

FIG. 2. Oceanic zonal monthly mean cloud type frequencies at 0730 LT in Jul 1987 (daylight on Northern Hemisphere) and in Jan 1988 (daylight on Southern Hemisphere). Cloud types are divided into four categories: high opaque, cirrus, midlevel, and low-level clouds identified by (a), (e) original 3I; (b), (f) current ISCCP (CX); (c), (g) reprocessed ISCCP (DX); and (d), (h) new 3I.

the cloud-top pressure category is determined by the average cloud-top pressure within the grid. For both cases, if the average visible optical thickness τ is <9.4, or the cloud cover is <0.5 (for midlevel and lowlevel clouds), then the ISCCP clouds are classified in the lower opacity category (Table 2). Both schemes lead to nearly the same most frequent cloud-type maps. Therefore we show ISCCP results only for the first scheme.

The reprocessed ISCCP dataset (DX) shows an improved identification of cirrus (in daytime summer), leading to better agreement with the 3I cloud parameters (Fig. 1). At night however, 3I provides superior cirrus information to the ISCCP results. Note that at 0730 LT there is daylight only in the summer hemisphere. In July there are mostly cirrus over the Northern Hemisphere land, whereas in winter these regions are more frequently covered by midlevel and low clouds. In general, the 3I cirrus zone around the intertropical convergence zone (ITCZ) is broader in meridional extent than the DX cirrus zone.

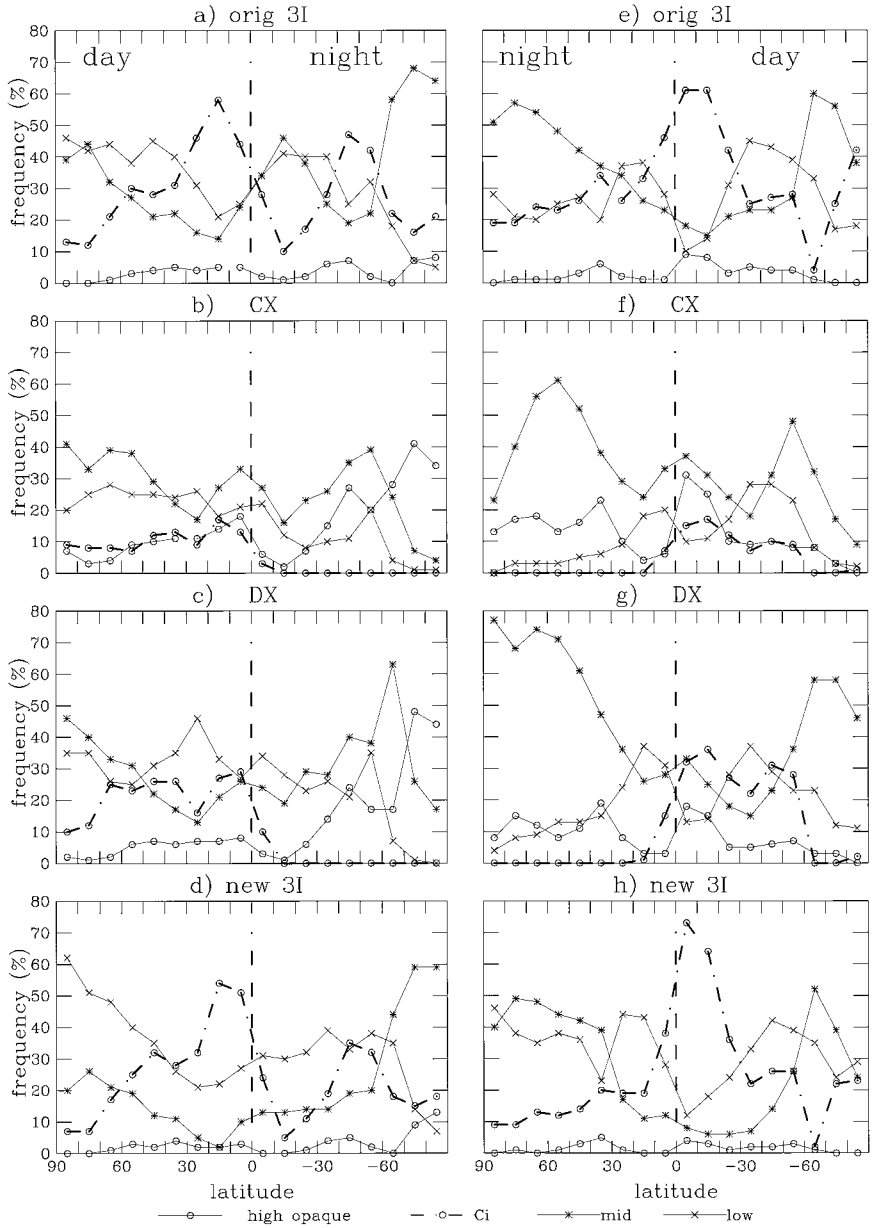

FIG. 3. Terrestrial zonal monthly mean cloud type frequencies at 0730 LT in Jul 1987 (daylight on Northern Hemisphere) and in Jan 1988 (daylight on Southern Hemisphere). Cloud types are divided into four categories: high opaque, cirrus, midlevel, and low-level clouds identified by (a), (e) original 3I; (b), (f) current ISCCP (CX); (c), (g) reprocessed ISCCP (DX); and (d), (h) new 3I.

With 3I, one can recognize the Southern Hemisphere storm track zone and the Northern Atlantic storm track in winter. During summer, these zones are covered mostly by midlevel and low-level clouds. The earth's deserts are cloudier in July than in January according to 3I, in agreement with climatological surface observations by Warren et al. (1986). When there are clouds, they are mostly cirrus in summer, but a mixture of low clouds and cirrus in winter. ISCCP finds a predominance of low clouds in summer, but clear sky and cirrus in winter. The more prevalent cumulus clouds in summer in the ISCCP results may arise from its detection of dust storms. Marine stratus clouds appear more often in DX than in CX data for these particular months because of an improvement of the visible reflectance calibration: higher *NOAA-10* visible reflectances lead to higher optical thickness and therefore to lower clouds in the ISCCP algorithms. These stratus clouds are also much better identified by the new-3I cloud scheme, whereas the original 3I cloud scheme misidentified clouds in the

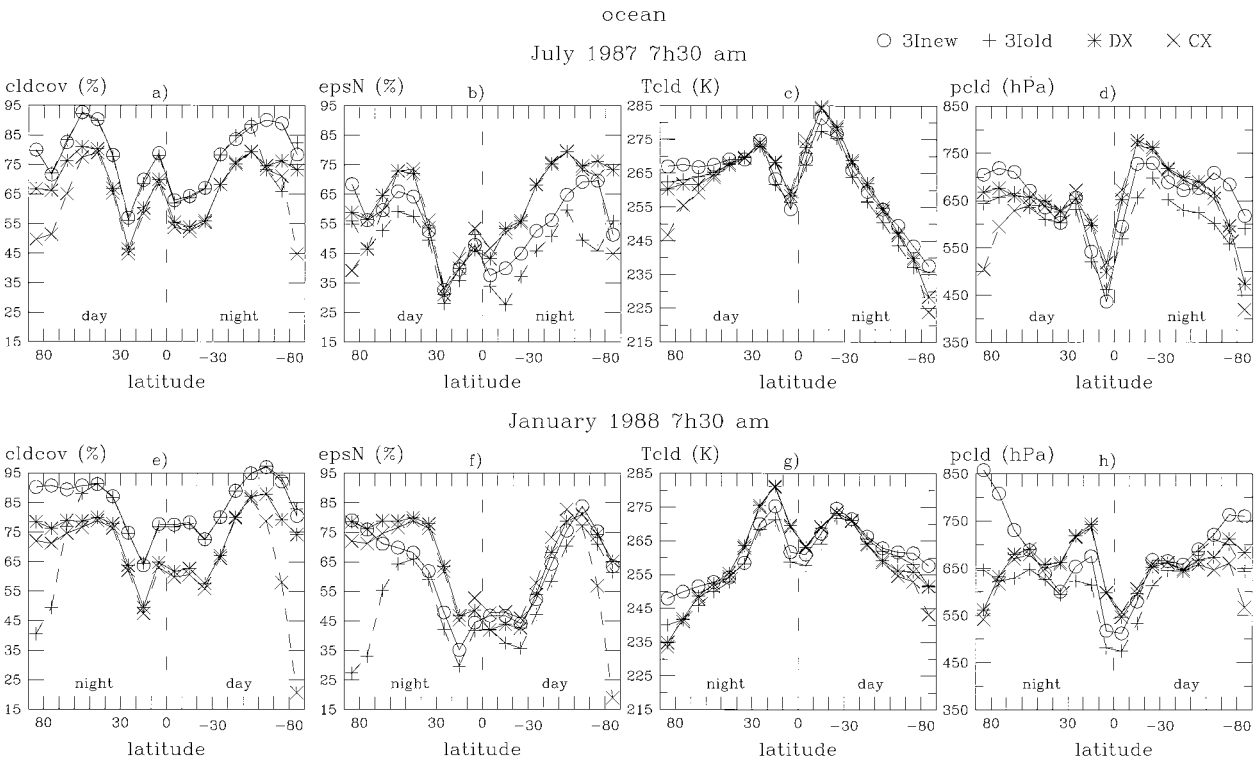

FIG. 4. Oceanic zonal monthly means of cloud cover, effective cloud amount, cloud-top temperature, and cloud-top pressure, at 0730 LT in Jul 1987 [(a)–(d) daylight on Northern Hemisphere] and in Jan 1988 [(e)–(h), daylight on Southern Hemisphere]. Compared are cloud parameters determined by original 3I, current ISCCP (CX), reprocessed ISCCP (DX) and new 3I.

marine stratocumulus regions off the western coasts of California, South America, Namibia, and Australia as thin midlevel clouds and underestimated their areal cover. An interesting feature is the appearance of cirrus clouds off the eastern North American coast in July, which is confirmed by the HIRS analysis of Wylie and Menzel (1999), but not as well identified by ISCCP in the morning hours. A possible reason for this difference could be that low-level clouds lie underneath these cirrus, so that ISCCP would have difficulties identifying them correctly (Jin and Rossow 1997). All the other oceanic regions are covered mostly by low opacity, low-level clouds (i.e., cumulus).

b. Zonal distributions of cloud parameters

The study of cloud type frequencies can be carried out further by considering monthly averaged zonal-mean cloud type frequencies, in section 3b(1). We then compare directly the different cloud parameters such as cloud cover, cloud opacity, and cloud-top pressure in sections 3b(2) to 3b(4). Their monthly averaged zonal-mean values, as obtained from orig-3I, CX, DX, and new-3I, are shown in Figs. 4 for ocean and in Figs. 5 for land, in July 1987 (a)–(d) and in January 1988 (e)–(h). For easier comparisons, the differences between new-3I and the other three results are also shown as a function of latitude in Fig. 6 for ocean and Fig. 7 for land.

Since at 0730 LT time only the summer hemisphere has daylight, we use the comparison with the ISCCP in the summer hemispheres to obtain a measure of the reliability of the 3I algorithms and use the comparison with ISCCP in the winter hemispheres to evaluate its biases when using only IR radiances (overall, ISCCP should overestimate cloud-top pressure and emissivity at night since all clouds are assumed to be blackbodies).

1) CLOUD TYPE FREQUENCIES

The orig-3I, new-3I, CX and DX zonal, monthly mean cloud type frequencies in Figs. 2 for ocean and Figs. 3 for land show that over ocean new-3I identifies about 10% more cirrus than DX in mid- and low latitudes, under daylight condition. Over tropical land the difference is even 20%. These cirrus clouds have been identified by ISCCP as midlevel clouds. Note the improvement of 10%–20% from CX to DX cirrus frequencies. Toward the poles ISCCP detects many more midlevel clouds than new-3I, which identifies more of these as low-level clouds. These different identifications arise from the different spatial and spectral resolutions (probably in the case of cirrus-midlevel cloud misidentification) as well as from different temperature profiles

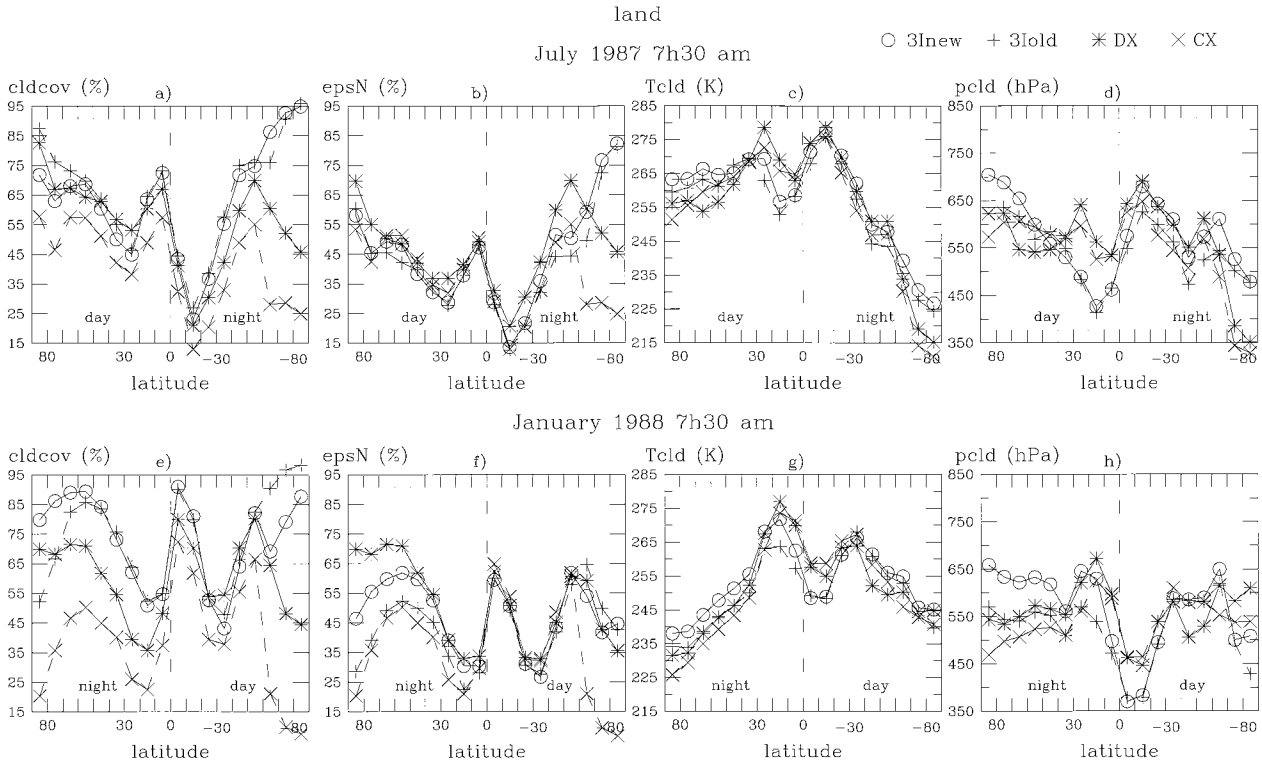

FIG. 5. Terrestrial zonal monthly means of cloud cover, effective cloud amount, cloud-top temperature, and cloud-top pressure, at 0730 LT in Jul 1987 [(a)–(d) daylight on Northern Hemisphere] and in Jan 1988 [(e)–(h) daylight on Southern Hemisphere]. Compared are cloud parameters determined by original 3I, current ISCCP (CX), reprocessed ISCCP (DX), and new 3I.

[probably in the case of midlevel–low-level cloud misidentification, see section 3b(4)]. Liao et al. (1995) have demonstrated that the tropical effect can be caused by the generally diffuse tops of high-level clouds, which produces a difference in the IR brightness temperature with wavelength. A second reason for different cloud identification can come from the perception of multilayer clouds. In Figs. 2 and 3, we use the first scheme for ISCCP cloud type identification, described in section 3a: the most frequent ISCCP cloud type inside a 1° grid. The second scheme, ISCCP cloud type identification from average cloud-top pressure, leads to slightly more midlevel clouds (less than 5% over ocean, 10% over polar land) and less cirrus (especially over Northern Hemisphere land) and low-level clouds, averaging the effect of multilevel clouds. In the case of homogeneous cloud scenes (the same cloud type in all ISCCP pixels within 1°), the difference decreases (see also paper 3).

2) CLOUD COVER

Cloud cover fraction of a 1° × 1° grid can be estimated in both datasets by counting the fractional number of cloudy pixels. Since the HIRS pixel size is about three to four times larger than the AVHRR pixel, HIRS estimates should generally overestimate cloud cover fraction somewhat relative to AVHRR, if the detection sensitivity is the same (Wielicki and Parker 1992; Rossow et al. 1993). However, we expect the detection sensitivity of HIRS to exceed that of AVHRR for optically thin, high-level clouds (cf. Jin et al. 1996), which will further enlarge the differences.

Over ocean, the CX and DX cloud cover fractions are nearly identical equatorward of 50° because there was no significant change in cloud detection algorithm; a small increase of low-level cloudiness is caused by changing from a radiance to a reflectance threshold, which is equivalent to a small decrease in the average threshold magnitude (Rossow et al. 1996). At higher latitudes, the DX cloud cover has been increased by use of an additional 3.7-μm threshold test for cloud detection (day and night), improving the agreement with new-3I cloud cover. The refinement of the HIRS brightness temperature calibration compared to radiosonde measurements in the new-3I scheme also produced an increase of polar cloud cover (ocean and land) in winter by 0.20–0.50, relative to orig-3I, improving the comparison with ISCCP. The AVHRR–HIRS spatial resolution effect explains only a part of the overall 0.10 higher cloud cover fraction for the new-3I compared with DX in July 1987 (Figs. 4a and 6a) and in January (Figs. 4e and 6e) where the difference approaches 0.15. Jin et al. (1996) estimated that the HIRS–AVHRR resolution differences of cloud fraction were only about 5%, consistent with Wielicki and Parker (1992) that

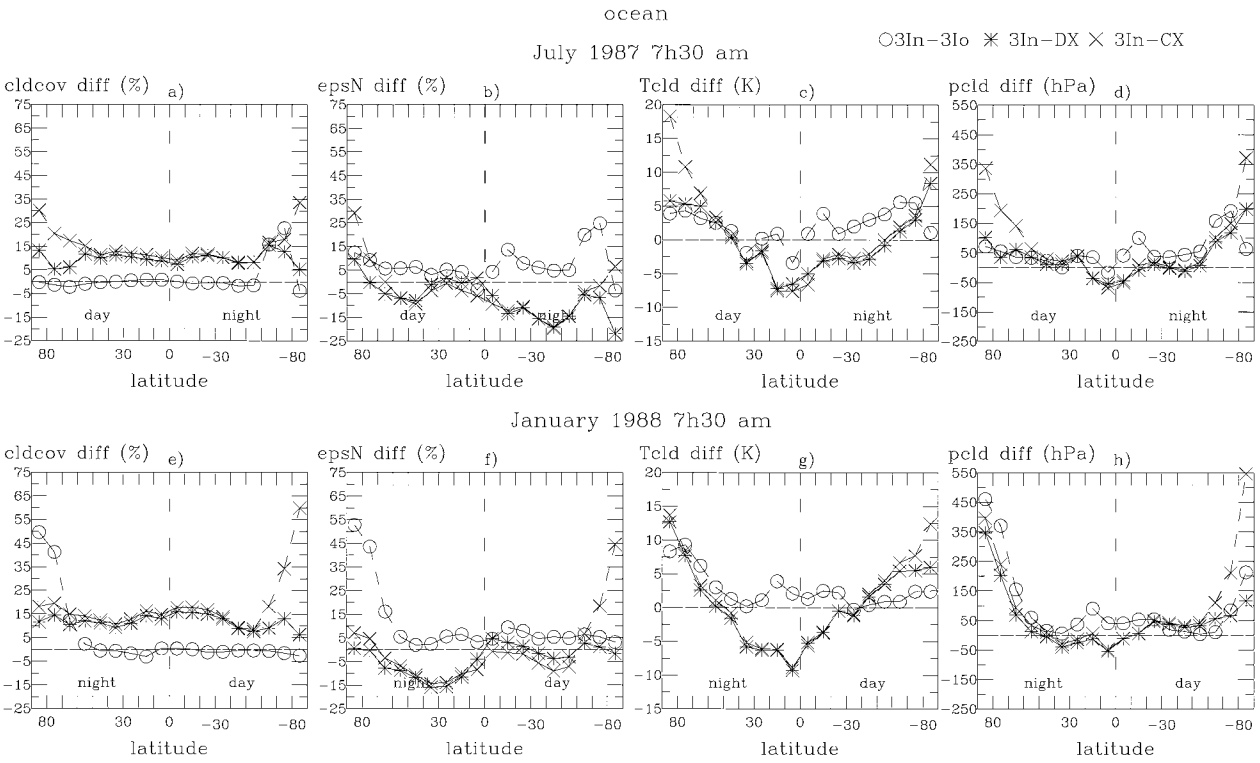

FIG. 6. Oceanic zonal monthly mean differences of cloud cover, effective cloud amount, cloud-top temperature, and cloud-top pressure between new 3I and original 3I, between new 3I and current ISCCP (CX), and between new 3I and reprocessed ISCCP (DX), at 0730 LT in Jul 1987 (a)–(d) and in Jan 1988 (e)–(h).

show about 5% increases with doubling of pixel sizes from 2 km to 8 km. The remaining difference is produced by the detection of more thin cirrus by 3I than ISCCP (cf. Jin et al. 1996; Liao et al. 1995; Menzel et al. 1992).

Over land, the DX cloud cover increased by about 0.10 relative to the CX cloud cover because the IR radiance thresholds were lowered and by about 0.25 over the summertime polar regions because of lowered thresholds and the additional use of the 3.7-μm threshold. This leaves a 0.05–0.10 difference between 3I and DX cloud cover in the daytime hemisphere, slightly smaller than the difference over the oceans. Note that with the algorithm changes, new-3I and DX now differ by a similar amount over the whole globe that can be explained by the resolution effect and differing detection sensitivity. The exception occurs over the deserts (around 35°N and 35°S), where the DX cloud cover may be overestimated by the IR threshold change (Figs. 5a and 7a). The 3I and CX clear sky statistics over the Sahara region are nearly the same, whereas in the DX dataset two-thirds of the clear sky are identified now by very thin low-level clouds. The IR temperature variability within 1° of 3I, CX, and, respectively, DX scenes is nearly identical with 0.7, 0.9, and, respectively, 0.8 K for clear sky; 2.0, 1.6, and, respectively, 1.5 K for low clouds; and 6.3, 7.3, and, respectively, 8.1 K for high clouds. Only the statistics of these scenes are very different, indicating a smooth transition from completely clear to cloudy, but the clear/cloudy decision makes the cloud cover jump. One explanation of these ''extra'' clouds in ISCCP might be given by dust storms occuring in summertime. In new-3I, the elimination of the albedo test over polar land and the maximum value test over land with topography variations >250 m has produced a small decrease of total cloud cover over land. Over Antarctica the disagreement with ISCCP is still about 0.40: new-3I shows nearly complete overcast. The difference appears mainly over the high plateau in eastern Antarctica where ISCCP reports mostly clear sky and new-3I reports mostly overcast semitransparent cirrus. Even with the improvement of the ISCCP cloud cover, there still seems to be an underestimate of total cloud cover over land during nighttime.

Both 3I and ISCCP indicate the main cloudy zones and their seasonal changes (Figs. 4 and 5). The ITCZ is located more over ocean in July and more over land in January. The ITCZ cloud cover maximum is divided from the midlatitude storm track maxima by the subtropical subsidence zones where cloud cover reaches a minimum. The standard deviation of monthly mean cloud cover in each latitude band (not shown), indicating longitudinal variations, decreases from 0.40 to 0.10 with decreasing mean cloud cover for new-3I; the ISCCP results show a similar pattern with somewhat less variation (peak standard deviations between 0.30 to 0.40).

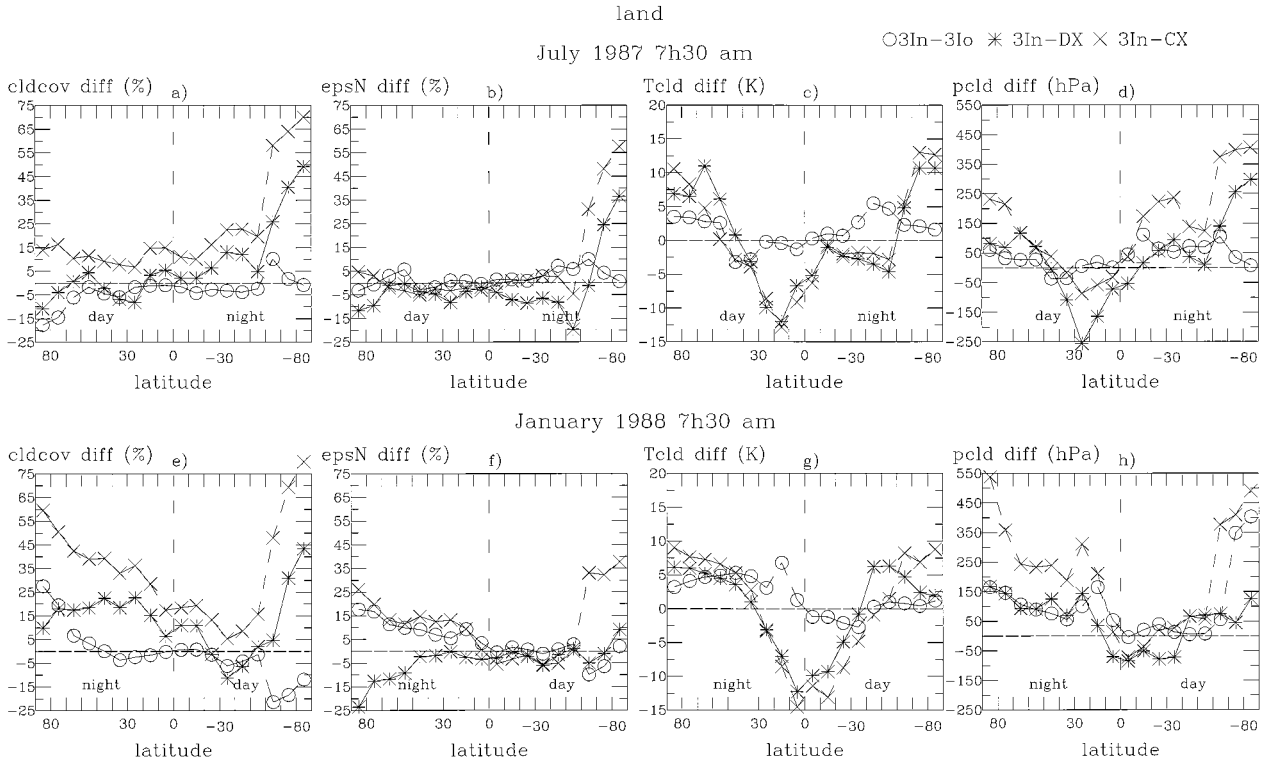

FIG. 7. Terrestrial zonal monthly mean differences of cloud cover, effective cloud amount, cloud-top temperature, and cloud-top pressure between new 3I and original 3I, between new 3I and current ISCCP (CX), and between new 3I and reprocessed ISCCP (DX), at 0730 LT in Jul 1987 (a)–(d) and in Jan 1988 (e)–(h).

3) EFFECTIVE CLOUD AMOUNT

Effective cloud amount over a 1° grid is the product of the cloud cover fraction and the IR emissivity of the clouds. This quantity is calculated by the 3I cloud scheme as the product of fraction of cloudy HIRS pixels within a 1° grid and the effective cloud amount obtained from the average radiances of all cloudy pixels.

ISCCP determines cloud optical thickness, τ, from the measured visible radiance for each cloudy pixel only during day. To transform optical thickness into IR cloud emissivity, we use the following formula on each ISCCP pixel: $\varepsilon = 1 - \exp(-\tau/b)$, where b relates the optical thickness from the VIS to the IR domain; it depends on the cloud phase: $b = 2.13$ for ice clouds and $b = 2.56$ for liquid clouds (Rossow et al. 1996). We calculate the average IR cloud emissivity at a spatial resolution of 1° by first transforming optical thickness into IR cloud emissivity for each pixel and then averaging the IR cloud emissivities over the cloudy pixels inside a 1° grid. This method is the most appropriate for a comparison with 3I (paper 3). In the collocated ISCCP–3I dataset, optical thickness and IR emissivity are determined at the same viewing zenith angle (since AVHRR and HIRS are on the same satellite). To obtain the ISCCP effective cloud amount, the averaged IR cloud emissivity is then multiplied by the ISCCP cloud cover fraction.

The behavior of the zonal-mean effective cloud amounts (Figs. 4b and 5b) essentially follows that of cloud cover. Note that the effective cloud amount in the ITCZ has decreased by 0.05 going from CX to DX because the new treatment of ice clouds lowers the average emissivity. With the exception of the southern polar regions, where the 3I cloud cover is much larger than the DX cloud cover, the orig-3I effective cloud amount is generally 0.05–0.10 smaller than the DX effective cloud amount, unlike the cloud cover, which is about 0.10 larger. By looking at geographical maps (Fig. 7b in paper 2), the orig-3I effective cloud amount is especially small in regions dominated by low-level clouds, most dramatically in the marine stratocumulus regions off the west coasts of the continents.

The new-3I cloud scheme increases the effective cloud amount in these regions (Fig. 8b in paper 2), leading to an overall good agreement between new-3I and DX in the daytime hemisphere. That the slightly larger cloud cover fraction determined by 3I is offset by a slightly smaller cloud emissivity supports the interpretation that these differences are associated mostly with the difference in detection sensitivity, reinforced by the smaller resolution effects. Only regions with a larger disagreement in cloud cover fraction still have a significant disagreement in effective cloud amount. At night, the DX effective cloud amount equals the cloud cover fraction, leading to an overestimate relative to

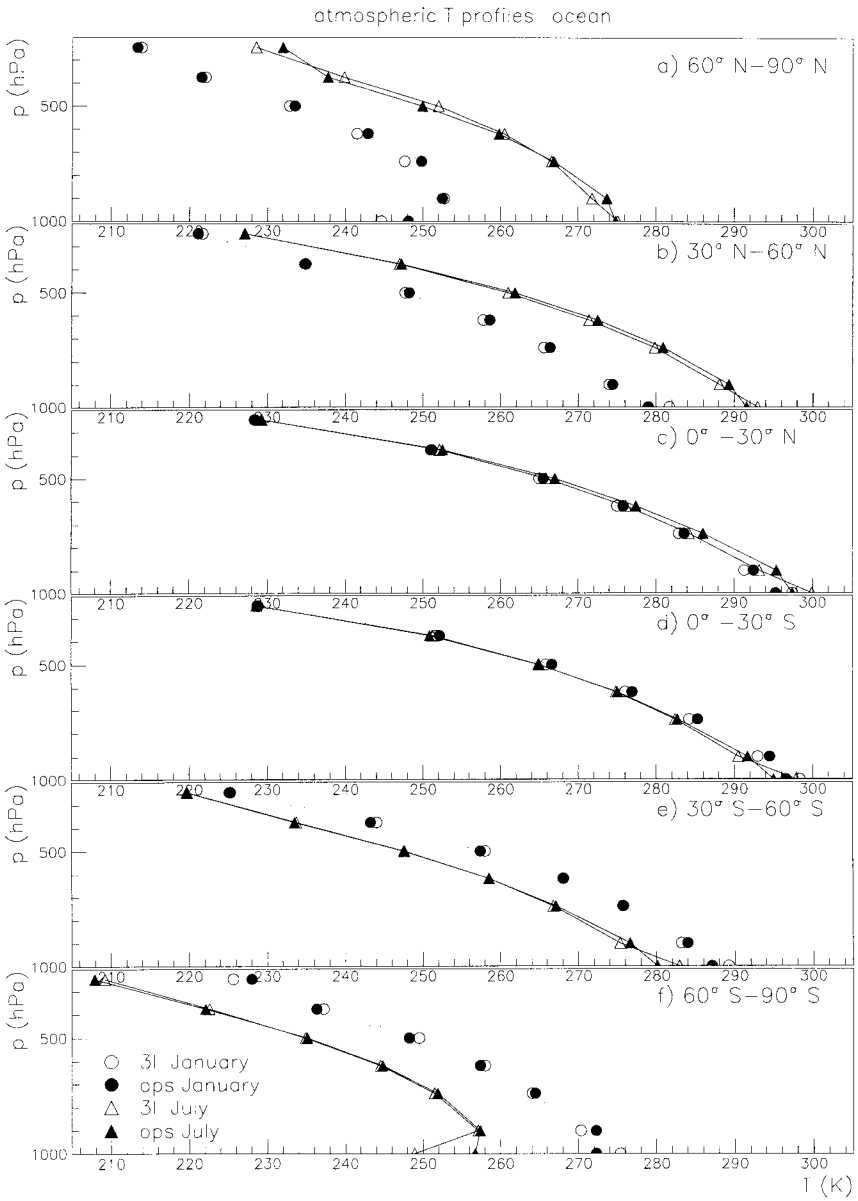

FIG. 8. Oceanic monthly mean atmospheric temperature profiles as determined by 3I and by operational TOVS, in six 30° wide latitude bands: (a) 60°–90°N, (b) 30°–60°N, (c) 0°–30°N, (d) 0°–30°S, (e) 30°–60°S, and (f) 60°–90°S in Jul 1987 and Jan 1988.

new-3I of 0.10–0.20, depending on the amount of cirrus clouds. The maximum difference can be seen in the winter midlatitude storm tracks over ocean.

4) CLOUD-TOP TEMPERATURE AND CLOUD-TOP PRESSURE

Colder-topped clouds predominate in the ITCZ and the polar regions and very warm-topped clouds predominate in the subsidence regions (Figs. 4c and 5c). The cloud-top temperature dispersion within a latitude band (not shown) is highest in the Tropics, due to the larger vertical extent of the troposphere, and generally decreases toward the poles. The average cloud-top temperature in the polar regions has increased from CX to DX by about 10 K, bringing it into better agreement with new-3I. This change is caused by the fact that the additional polar clouds detected in DX by lowered thresholds and the additional 3.7-μm test are all warmer than the clouds detected in CX. The new-3I cloud scheme increases the zonal mean 3I cloud-top temperature in regions with low-level cumulus clouds, in better agreement with DX.

Over desert in the summer hemisphere the zonal-

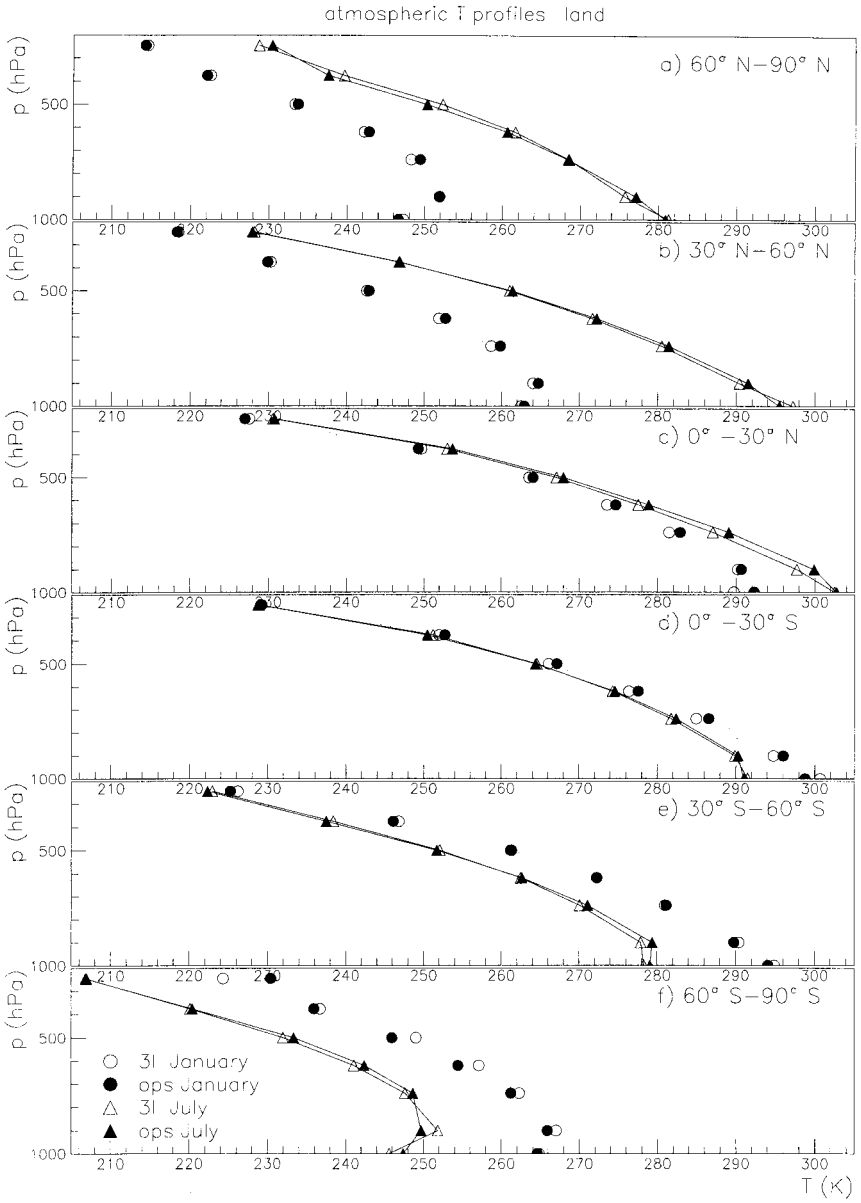

FIG. 9. Terrestrial monthly mean atmospheric temperature profiles as determined by 3I and by operational TOVS, in six 30° wide latitude bands: (a) 60°–90°N, (b) 30°–60°N, (c) 0°–30°N, (d) 0°–30°S, (e) 30°–60°S, and (f) 60°–90°S in Jul 1987 and in Jan 1988.

mean 3I cloud-top temperature is about 10 K lower than the one determined by DX (Figs. 5c and 5g). This can be explained by a disagreement between 3I and DX on the most frequent cloud type: new-3I indicates mostly cirrus, whereas DX indicates mostly cumulus. As discussed in section 3b(2), two-thirds of the DX cumulus clouds were in the clear sky category before. It is also possible that the cloud height correction of some of these clouds is not enough because of the relatively bright surface of the Sahara.

A systematic difference of cloud-top temperatures can be seen in Figs. 6c and 6g: new-3I clouds are colder than DX clouds in the Tropics and warmer than DX clouds toward the poles. However, this systematic variation is less noticeable when cloud-top pressures are compared (Figs. 6d and 6h). Some of these differences could be explained by a difference in cirrus identification [see section 3b(1)]. In the following we analyze the possibility of systematic differences in the atmospheric temperature profiles between 3I and the operational TOVS analysis used by ISCCP.

The zonal, monthly mean 3I and operational TOVS atmospheric temperature profiles (surface temperature and six-layer-mean temperatures), as well as their dif-

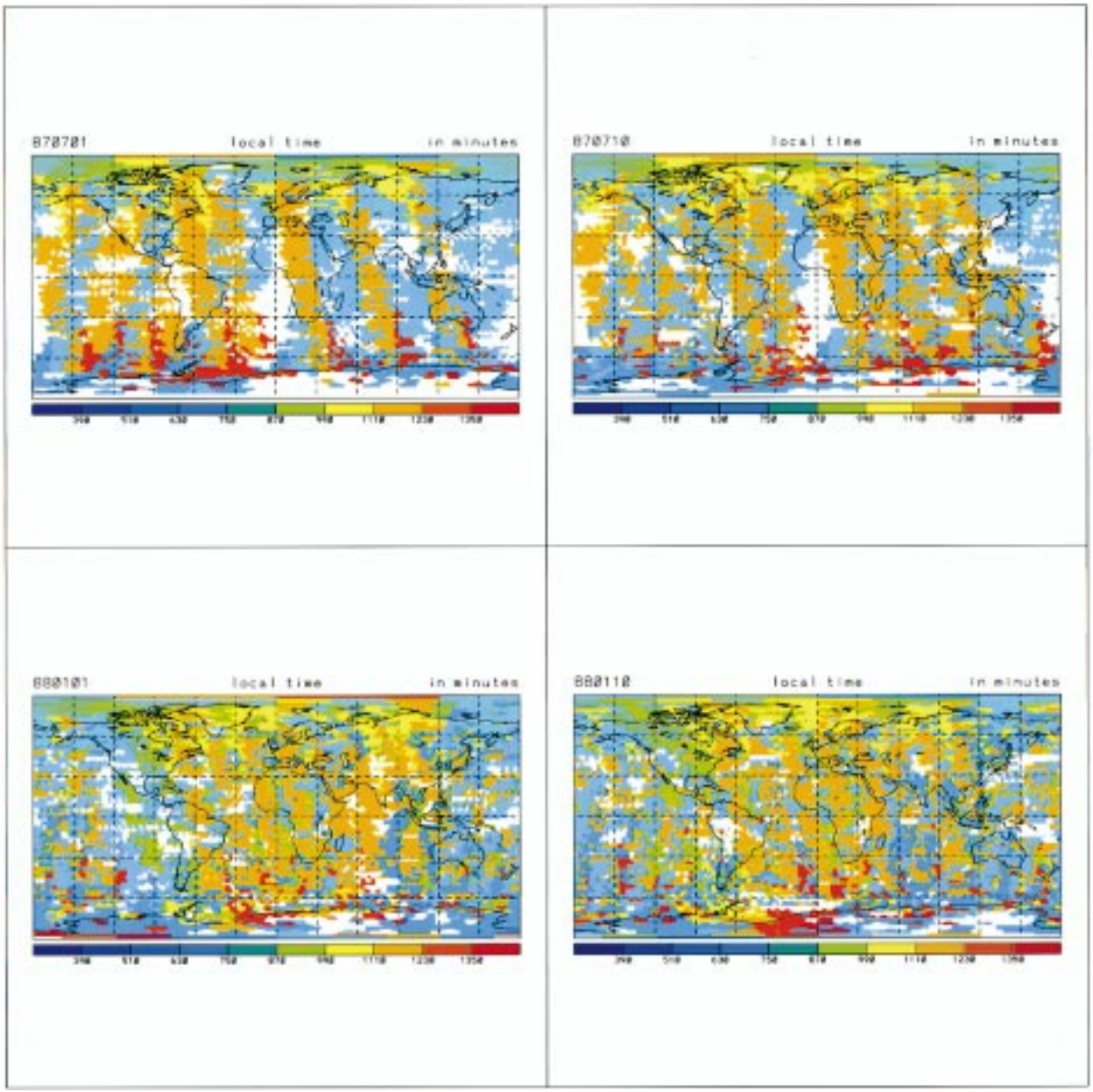

FIG. 10. Geographical maps with local observation times of the operational TOVS temperature profiles provided to ISCCP, for two days in Jul 1987 (a) and (b) and for two days Jan 1988 (c) and (d).

ferences, are shown in Figs. 8a–f for ocean and in Figs. 9a–f for land, for six different latitude bands of 30° width. For an exact comparison, the 3I atmospheric temperature layers were interpolated to the layers used by ISCCP: surface to 800, 800–680, 680–540, 540–440, 440–330, and 330–200 hPa. In general, the form of the 3I and operational TOVS temperature profiles agrees quite well, but the 3I temperature profiles are slightly colder in the lower atmosphere and the same or slightly warmer at higher latitudes in the upper atmosphere than the operational TOVS temperature profiles used in ISCCP.

With the exception of polar winter (sea ice), the SST determined by 3I is about 1–3 K warmer than the one determined by operational TOVS; the ISCCP retrievals of surface temperature are similarly warmer than the TOVS values. Over land, the effect is less systematic. At the early morning overflight time of *NOAA-10*, the surface temperatures retrieved by ISCCP are also similar to the operational TOVS values, except for some mountainous regions (cf. Jin et al. 1996). The operational TOVS lower-atmospheric temperature profiles over land and ocean look much more alike, with the exception of midlatitude land in winter, where one observes a tem-

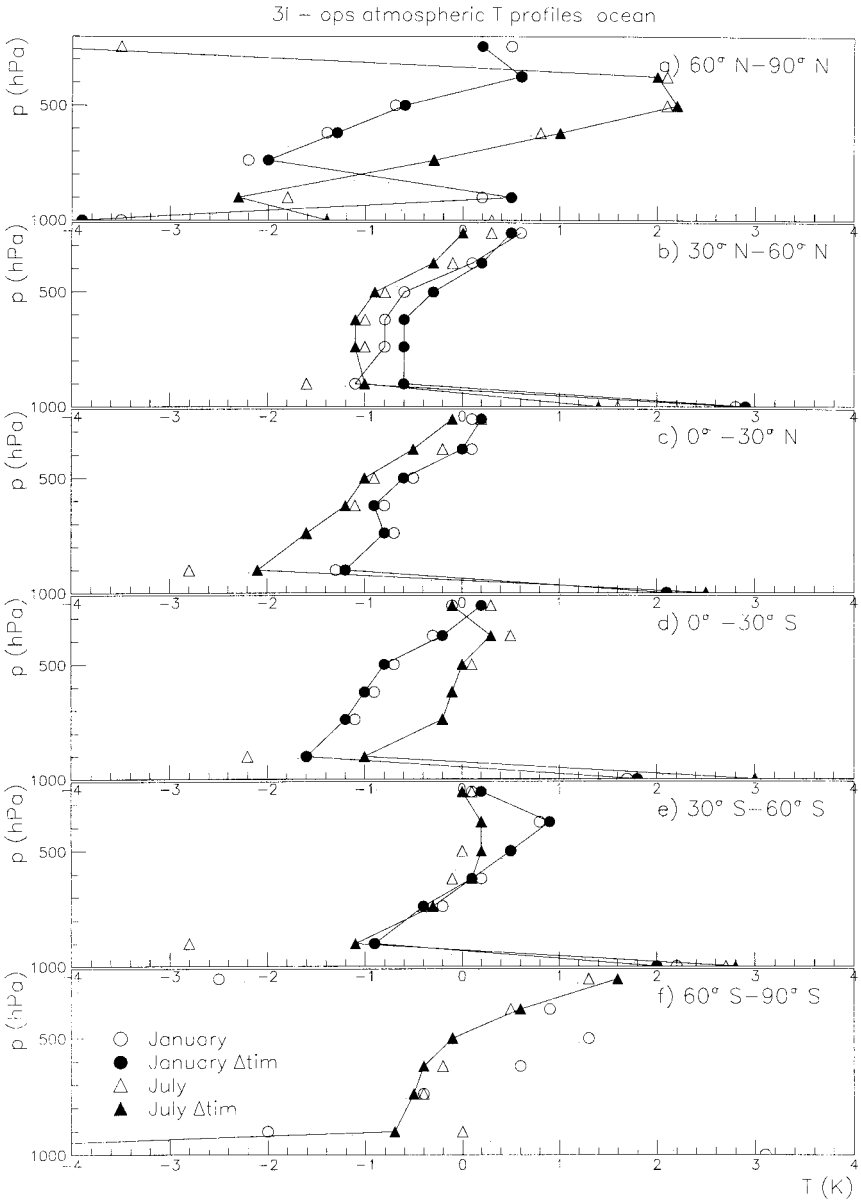

FIG. 11. Oceanic monthly mean atmospheric temperature profile differences between 3I and operational TOVS in six 30° wide latitude bands: (a) 60°–90°N, (b) 30°–60°N, (c) 0°–30°N, (d) 0°–30°S, (e) 30°–60°S, and (f) 60°–90°S in Jul 1987 and Jan 1988. Compared are differences including all measurements and differences including only time-matched measurements (Δtim).

perature inversion. The 3I lower atmospheric temperature profiles, however, show a smaller temperature gradient over land than over ocean, especially in the Tropics.

One difference in the atmospheric temperature profiles used for cloud parameter determination by 3I and ISCCP comes from the fact that operational TOVS provides temperature profiles to ISCCP only *once per day*, extracted at different times from the four daily measurements (0730 and 1930, 0230 and 1430 LT). If no operational TOVS information is available, ISCCP uses values from a climatology. The 3I determines the atmospheric temperature profile at the same time that the clouds are observed, or in case of failure, a first guess profile from the TIGR dataset is used instead. Geographical maps with local observation times of the operational TOVS atmospheric temperature profiles provided to ISCCP are shown in Fig. 10, for 2 days in July and 2 days in January. In July, observations come from the same satellite, but morning and evening observations alternate every second orbit. In January, observations from the *NOAA-9* satellite have also been introduced. These time differences should affect the atmospheric temperature profiles, especially over land.

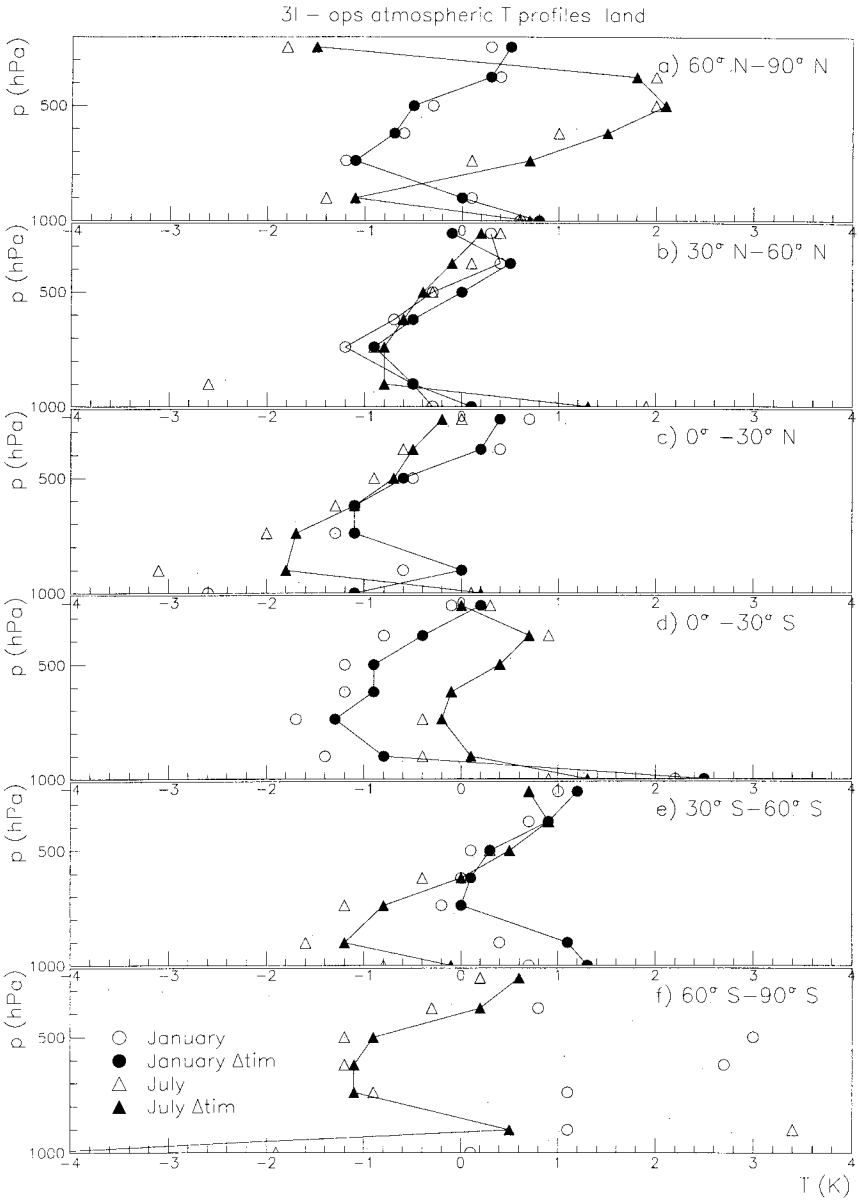

FIG. 12. Terrestrial monthly mean atmospheric temperature profile differences between 3I and operational TOVS in six 30° wide latitude bands:(a) 60°–90°N, (b) 30°–60°N, (c) 0°–30°N, (d) 0°–30°S, (e) 30°–60°S, and (f) 60°–90°S in Jul 1987 and Jan 1988. Compared are differences including all measurements and differences including only time-matched measurements (Δtim).

But also different cloud cover situations at the different observation times can affect the atmospheric temperature profiles, and these again influence the determination of cloud parameters.

Zonal, monthly mean differences between 3I and operational TOVS atmospheric temperature profiles are shown in Figs. 11 (ocean) and 12 (land) for all 3I–ISCCP observations and for 3I–ISCCP observations that have atmospheric temperature profiles observed approximately at the time (within 1 h). Indeed, when the time differences are reduced, the temperature profiles agree somewhat better, especially in the 900-hPa layer for land, and in this layer also for ocean. In the case where no operational TOVS information is available, disagreements between ISCCP and 3I temperatures become larger (not shown).

Figures 11 and 12 show that ISCCP cloud-top temperatures of high-level clouds in the Tropics or of mid-level clouds at higher latitudes would be converted into a larger cloud-top pressure (lower clouds) by using the 3I atmospheric temperature profile. This effect does not exceed 50 hPa on a monthly average, but would affect the cloud type comparisons somewhat. It will be studied in more detail for some regions in section 4. Since we

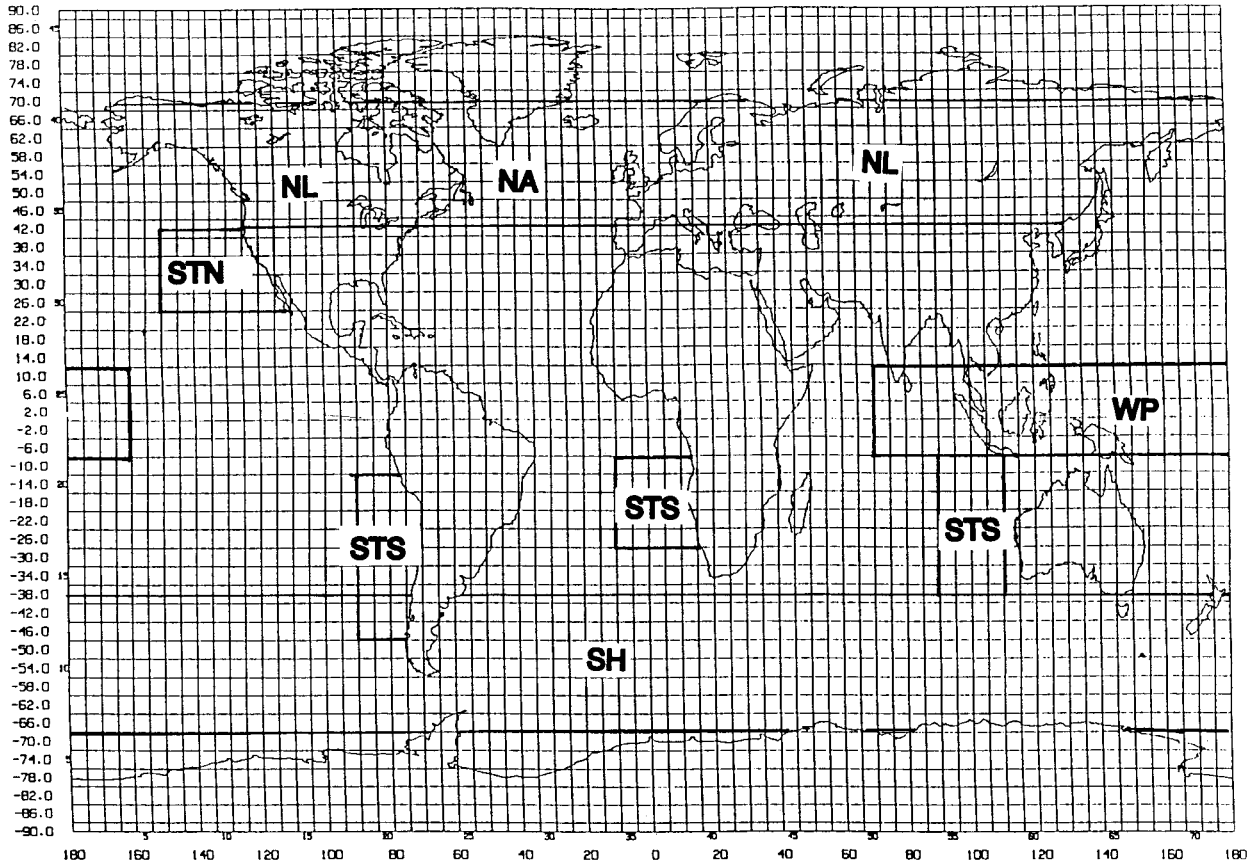

FIG. 13. Geographical regions used for the regional analyses: northern midlatitude land (NL); North Atlantic (NA); Southern Hemisphere midlatitude ocean (SH); marine startocumulus regions off the western continental coasts near California (STN) and near Peru, Namibia, and Australia (STS); and tropical warm pool near Indonesia (WP).

have focused our discussion so far on comparisons in the summer hemisphere, we see from Figs. 11 and 12 that the temperature discrepancies are larger in summer than in winter, suggesting that some of the temperature profile differences are associated with different water vapor treatments by the operational TOVS and 3I analyses.

4. Regional comparisons

Since the variability within latitude zones can be quite large and global maps have a more qualitative than quantitative character, we have selected several geographical regions encompassing the main climatological regimes for more detailed quantitative comparisons. These regions are indicated in Fig. 13: 1) Northern midlatitude (40°–70°N) land (NL) containing the North American continent as well as Europe, the southern part of Greenland, and the Northern half of Asia; 2) North Atlantic (40°–70°N; NA), ocean between North America and Europe; 3) Southern Hemisphere midlatitude (40°–70°S) ocean (SH), the only regions excluded in this zone are New Zealand and the Southern part of South America; 4) the marine stratocumulus regions off the western continental coasts (ST), including (a) STN near California (20°–40°N) in July and (b) STS near Namibia (10°–30°S), Australia (10°–40°S), and South America (15°–50°S) in January; and (5) the tropical ''warm pool'' near Indonesia continuing eastward (10°S–10°N, 70°E–160°W) (WP).

In the following we focus on four cloud types: cumulonimbus (high-level, high opacity clouds), cirrus (high-level, low opacity clouds), and midlevel and low-level clouds (the latter two categories include clouds of all opacities). The ISCCP results classified by the most frequent cloud type within a 1° grid and by the type associated with the average cloud properties differ only slightly, so we present only ISCCP results from the most frequent cloud type. We also focus only on DX and new-3I results

Figures 14a–j show very similar monthly mean frequencies of ISCCP and 3I cloud types during daytime (in summer hemispheres). During nighttime (in winter hemispheres), cirrus clouds are misidentified by ISCCP as midlevel or low-level clouds.

Whereas each dataset exhibits very similar monthly

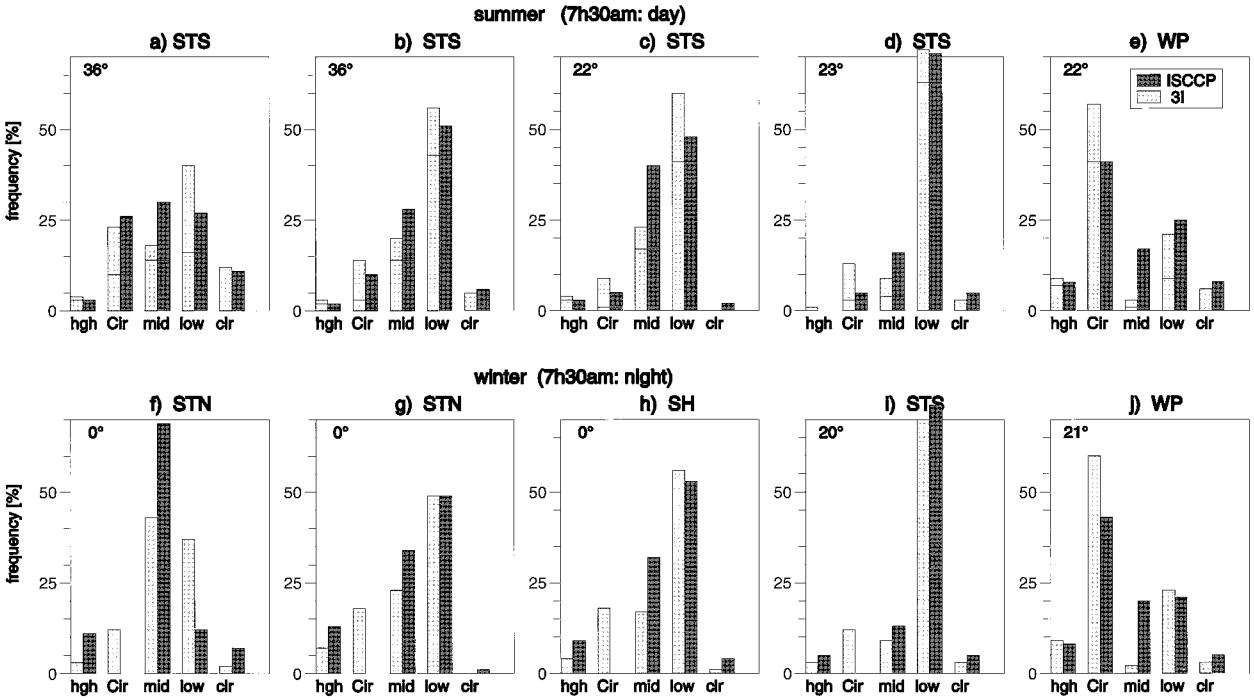

FIG. 14. Monthly mean cloud type frequencies in summer [(a)–(e) daylight] and winter [(f)–(j) night] over five geographical regions: (a), (f) Northern Hemisphere land; (b), (g) North Atlantic; (c), (h) Southern Hemisphere ocean; (d), (i) southern marine stratocumulus; and (e), (j) tropical warm pool. Cloud types are divided into four categories: high opaque, cirrus, and midlevel and low-level clouds identified by new 3I and reprocessed ISCCP. Monthly mean clear sky frequencies are also compared. In addition, the percentage of time–space collocated cloud type matching is indicated within each of the cloud type frequencies. For daylight situations, the mean sun elevation angle is indicated.

mean cloud type frequencies in these regions, direct comparison between simultaneous, collocated observations produces type matches only about 50% to 75% of the time. The percentage of cloud type matching is also indicated in Figs. 14a–e. Table 3 summarizes the total match-up frequencies in the six regions for both 3I cloud schemes. Improvement in cloud type matching with DX, going from orig-3I to new-3I, is found in all six geographical regions and varies from +6% (NL) to +27% (STN).

Considering that 3I cloud types are determined from parameters calculated once per 1° grid from the average radiances over all cloudy pixels (about 17 km × 17 km at nadir), whereas the ISCCP cloud types are determined by the most frequent cloud parameter values retrieved from radiances measured in smaller pixels (AVHRR measurements in GAC format correspond to about 1 km × 4 km at nadir, sampled to about 35-km spacing in satellite flight direction and 30-km spacing perpendicular to flight direction), direct comparisons are difficult (Fig. 15). Disagreements could be explained by the effects of cloud inhomogeneities (due to cloud sizes and multilayer clouds) within the 1° grid as well as within and among the different pixel sizes and spacings. This explanation is tested in two ways: 1) by repeating the match-up comparison using the ISCCP data to simulate

TABLE 3. Frequencies of time–space collocated cloud type matching agreement between 3I and ISCCP at 1° spatial resolution, in the six geographical regions illustrated in Fig. 13. Cloud type matching has been investigated between four categories: high opaque, cirrus, and midlevel and low-level clouds. Compared are 3I cloud types determined by the original 3I cloud scheme with reprocessed ISCCP cloud types, and 3I cloud types determined by the weighted-χ^2 method (new 3I) with reprocessed ISCCP cloud types. The ISCCP cloud type has been determined as the most frequent cloud type within 1°. New 3I cloud types are also compared to ISCCP cloud types determined from 1° averaged cloud parameters and to homogeneous ISCCP cloud types within 1°, which means the same cloud type out of the four defined above in all ISCCP pixels within the 1° grid.

Region	NL	NA	SH	STN	STS	WP
Orig-3I-ISCCP match	40.6%	46.2%	53.2%	49.5%	50.8%	47.5%
New-3I-ISCCP match, most frequent cloud type	47.4%	64.7%	64.1%	76.4%	72.8%	60.8%
Match, ISCCP cloud type from average parameters	46.0%	64.9%	64.7%	78.0%	73.4%	60.0%
Match, 100% ISCCP cloud type inside 1° grid	56.0%	82.2%	80.9%	87.1%	87.0%	68.4%

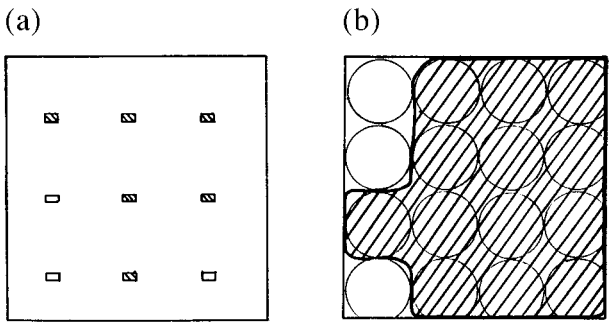

FIG. 15. Illustration of the spatial difference in ISCCP and 3I cloud observations. A 1° lat × 1° long grid box is filled (a) with approximately 1 km × 4 km large AVHRR pixels, which are sampled every 35 km in satellite flight direction and every 30 km perpendicular to flight direction and (b) with approximately 20 km × 20 km large HIRS pixels. Pixels detected as cloudy are hatched, for one example situation. In the case of ISCCP, cloud parameters are determined from each of these sampled observations, whereas 3I cloud parameters are determined over the mean radiances over the whole cloudy region.

3I as closely as possible by using the average cloud properties in each 1° to pick the cloud type, instead of the most frequent properties; and 2) by limiting the comparison to grids where the higher resolution ISCCP results are required to be homogeneous, defined by all individual pixels being the same cloud type (out of the four cloud types defined above). The match-up results are again displayed in Table 3. Results from averaged and most frequent ISCCP cloud properties are the same, but the cloud type matching increases by 10%–15% if one demands the same ISCCP cloud type within the 1° grid, leading to a final cloud type matching between 56% (NL) and 87% (ST).

Another analysis consists of studying cloud type characteristics: we examine the statistics of 1° gridboxes where 1) the cloud type identified by new-3I and DX is the same, 2) the cloud type is identified by DX but not by new-3I, and 3) the cloud type is identified by new-3I but not by DX. This analysis is limited to the four cloud types: high opaque, cirrus, midlevel, and low level.

Figures 16 to 19 give examples of cloud type characteristics in the different geographical regions. ISCCP cloud types are determined as the most frequent within 1°. In midlatitudes, the outgoing longwave flux (OLR) measured by ERBE (for more detail look at paper 3) over cirrus clouds is higher than the OLR over high opaque and midlevel clouds, but lower than the OLR over low-level clouds (Figs. 16a,b,e). In the Tropics, cirrus are thicker and hence the OLR over them is smaller (Fig. 16d). DX-only cirrus produce higher OLR, as high as that of low-level clouds. Also, the 3I-only and DX-only midlevel clouds have a higher OLR than midlevel clouds identified by both methods. The HIRS IR-window brightness temperature variance over cloudy pixels inside a 1° grid (Figs. 17a–e) is highest for cirrus identified by both methods, in agreement with an earlier study comparing 3I and AVHRR clouds (Stubenrauch et al. 1996). In comparison, the variance is much lower for DX-only cirrus, but as high as for DX-only low-level clouds, suggesting that these cirrus may be a misidentification of partly cloudy mid- or low-level clouds. This is confirmed from Figs. 18, which show that the ISCCP cloud cover is lower when 3I and ISCCP do not agree on the cloud type.

Figures 16 to 18 do not change much by calculating ISCCP cloud types from averaged quantities (not shown). By studying only homogeneous scenes (with the same cloud type in all ISCCP pixels within 1°), differences in cloud characteristics between 3I and ISCCP clouds appear mostly when the cloud cover is low (Figs. 18f–j). The DX cloud cover of ISCCP-only cloud types dropped by about 20% and of 3I-only cloud

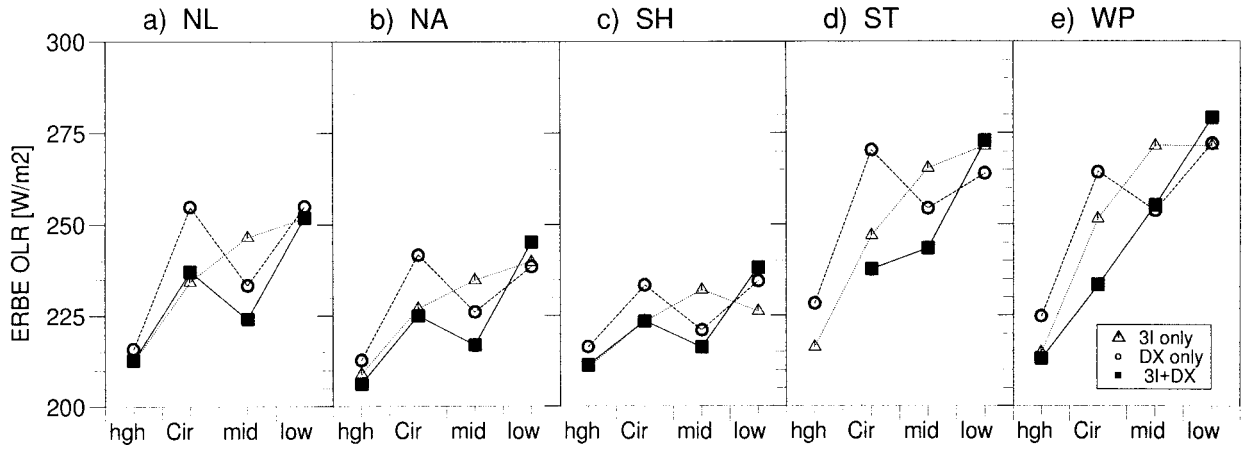

FIG. 16. Monthly mean ERBE outgoing LW flux (OLR) as a function of cloud type in five different geographical regions: (a) Northern Hemisphere land, (b) North Atlantic, (c) Southern Hemisphere ocean, (d) southern stratocumulus region, and (e) tropical warm pool. Cloud types are divided into four categories: high opaque, cirrus, and midlevel and low-level clouds. These cloud types have been identified simultaneously by 3I and ISCCP (■), only by ISCCP (○), and only by 3I (△).

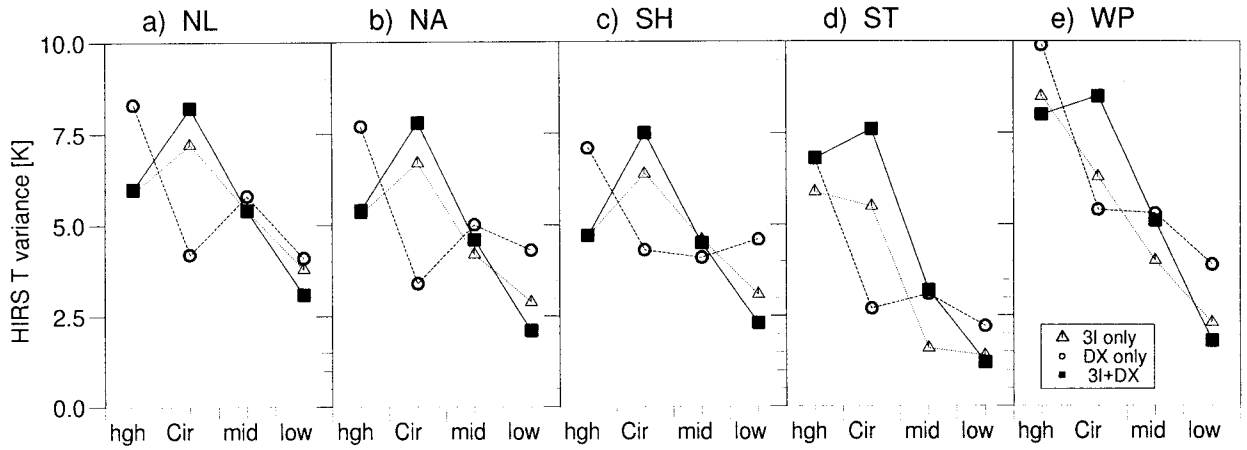

FIG. 17. Monthly mean cloudy HIRS IR window brightness temperature variance as function of cloud type in five different geographical regions: (a) Northern Hemisphere land, (b) North Atlantic, (c) Southern Hemisphere ocean, (d) southern stratocumulus region, and (e) tropical warm pool cloud types are divided into four categories: high opaque, cirrus, midlevel, and low-level clouds. These cloud types have been identified simultaneously by 3I and ISCCP (■), only by ISCCP (○), and only by 3I (△).

types by about 10%, confirming again that partly cloudy scenes are more difficult to identify correctly.

Discrepancies in the atmospheric temperature profiles can also cause differences in cloud classification. Figure 19 shows the monthly mean temperature differences between 3I and operational TOVS at six atmospheric levels for each cloud type. The temperature difference between 3I-only and ISCCP-only clouds can attain 2.5 K. The confusion between 3I and ISCCP low-level and midlevel clouds can be explained by this effect, espe-

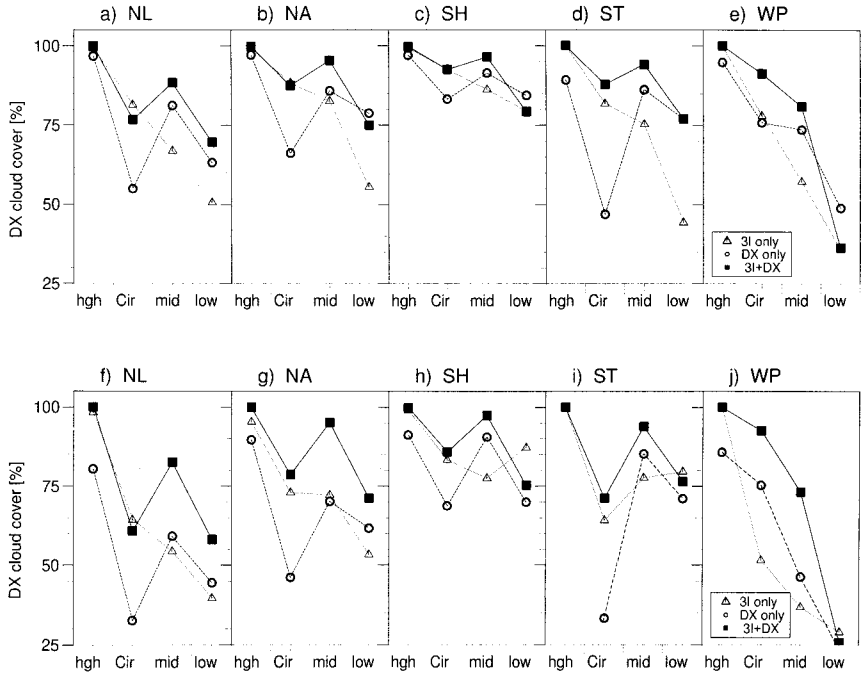

FIG. 18. Monthly mean ISCCP cloud cover as function of cloud type in five different geographical regions: (a), (f) Northern Hemisphere land; (b), (g) North Atlantic; (c), (h) Southern Hemisphere ocean; (d), (i) southern stratocumulus region; and (e), (j) tropical warm pool cloud types, which are divided into four categories: high opaque, cirrus, and midlevel, and low-level clouds. These cloud types have been identified simultaneously by 3I and ISCCP (■), only by ISCCP (○), and only by 3I (△). Panels (a)–(e) correspond to all situations, whereas (f)–(j) treat only homogeneous cloud scenes (with the same cloud type in all ISCCP pixels within a 1° grid box).

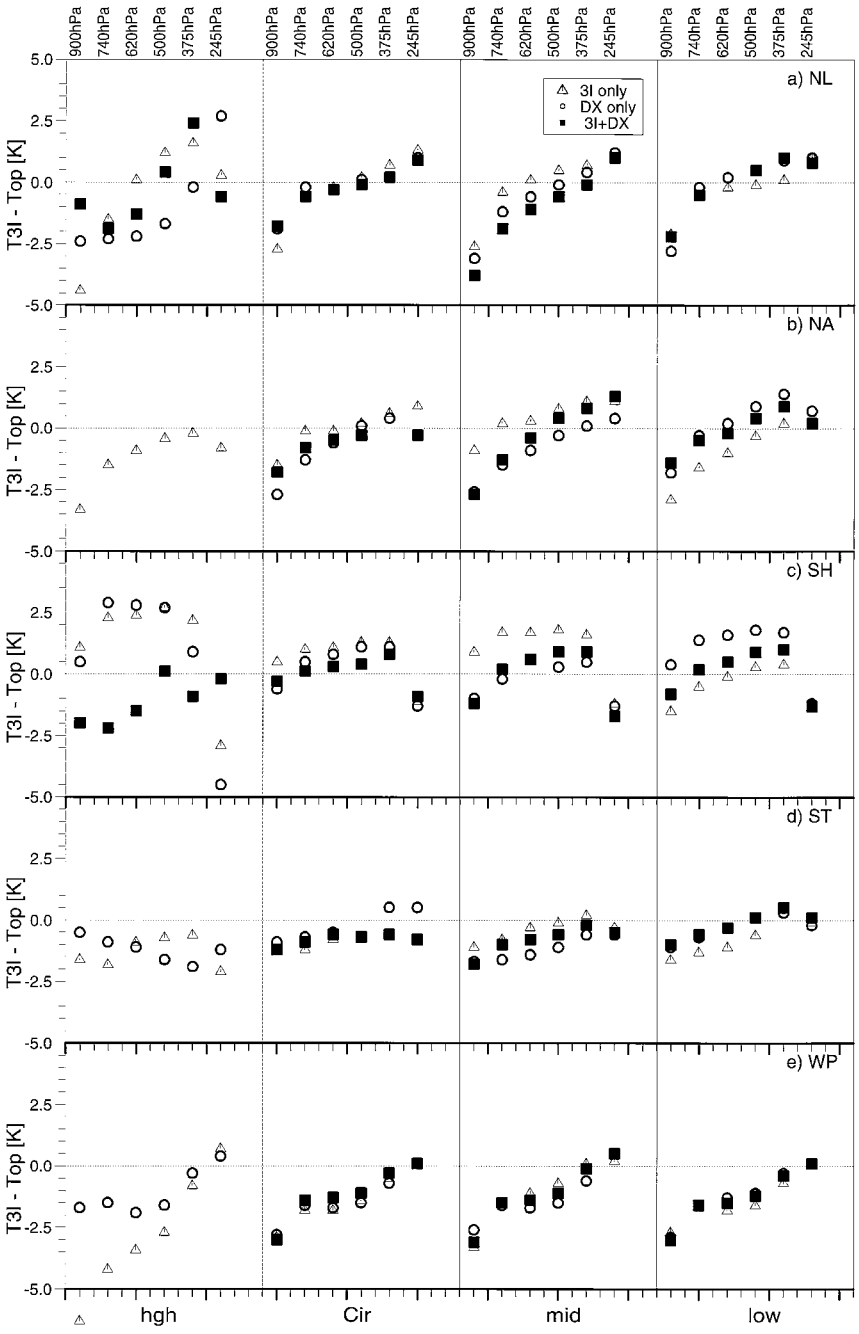

FIG. 19. Monthly mean temperature differences between 3I and operational TOVS at six atmospheric levels as function of cloud type, in five different geographical regions: (a) Northern Hemisphere land, (b) North Atlantic, (c) Southern Hemisphere ocean, (d) southern stratocumulus region, and (e) tropical warm pool. Cloud types are divided into four categories: high opaque, cirrus, and midlevel, and low-level clouds. These cloud types have been identified simultaneously by 3I and ISCCP (■), only by ISCCP (○), and only by 3I (△). Only homogeneous cloud scenes (with the same cloud type in all ISCCP pixels within 1° grid box) are considered.

cially over the Southern Hemisphere midlatitude ocean and the North Atlantic. The main reason for different cirrus identification seems not to be a different temperature profile, but lies more in the difficulty of cloud parameter determination in the case of partly cloudy scenes or multilayer clouds (see also paper 3).

If one does not want to consider cloud types anymore, another way to use combined information about both

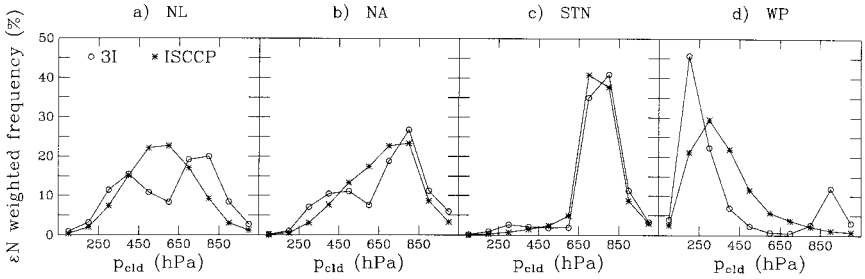

FIG. 20. Monthly mean effective cloud amount weighted cloud-top pressure distributions as determined by 3I (o) and by ISCCP (*) in four different geographical regions: (a) Northern Hemisphere land, (b) North Atlantic, (c) northern stratocumulus region, and (d) tropical warm pool.

cloud parameters, height and opacity, is to compare effective-cloud-amount-weighted cloud-top pressure distributions. These are shown in Figs. 20a–d, as obtained by ISCCP and 3I, for four different geographical regions. The 3I distributions show a bimodal structure with peaks around high- and low-level clouds, in agreement with observations by Susskind et al. (1997). The heights of these peaks depend very much on the geographical region. ISCCP produces distributions with one broad maximum. Before coming to conclusions, one has to be careful about systematic atmospheric temperature profile differences as discussed in Figs. 11 and 12. By considering cloud-top pressure distributions, the operational TOVS profiles are included in order to transform the measured ISCCP cloud-top temperature into a cloud-top pressure. On the other hand, if one considers cloud-top temperature distributions, the 3I atmospheric temperature profiles are included to transform the 3I-determined cloud-top pressure into cloud-top temperature. Indeed, the effective-cloud-amount-weighted cloud-top temperature distributions determined by 3I and ISCCP in Figs. 21a–d agree much better. Remaining differences in the midlatitudes can be accounted for by lower $N\varepsilon$ from 3I at lower temperatures due to heterogeneous regions (see paper 3) and in the tropical ''warm pool'' where one expects to encounter low-level clouds underneath cirrus clouds about 30% of the time (Jin and Rossow 1997), which ISCCP misidentifies as partly cloudy low-level clouds.

5. Conclusions

Comparison of space–time collocated 3I and ISCCP cloud parameters, obtained each from two different versions of algorithms, have given an evaluation of the improvement of these datasets. The recently reprocessed ISCCP dataset shows an improved cirrus identification during day, in better agreement with the 3I cloud classification. Additional cirrus information during night is provided by the 3I cloud scheme. The 3I identification of high and low clouds is equally reliable, by using the newly developed weighted-χ^2 method. Cirrus over low clouds seem to be better detected by 3I than by ISCCP. Within most geographical regions, the occurrence of cloud types identified by ISCCP or by 3I is the same. In spite of the different data and methods, the time–space collocated 3I–ISCCP cloud type matching reaches 76% in the stratocumulus regions. Over Northern Hemisphere land, where surface variabilities are higher, there is a 47% matching. These matchings improve further to

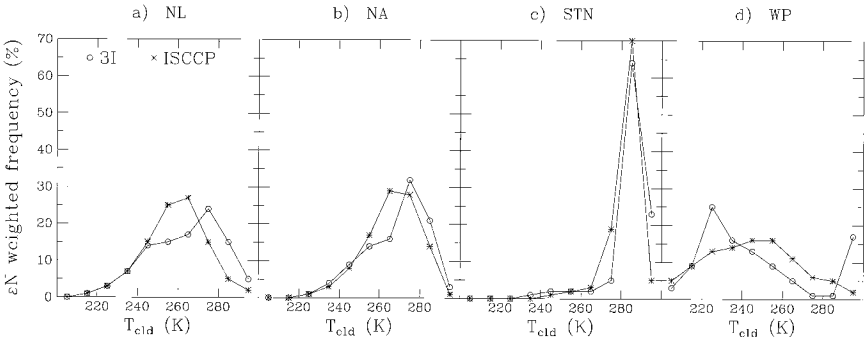

FIG. 21. Monthly mean effective cloud-amount-weighted cloud-top temperature distributions as determined by 3I (o) and by ISCCP (*) in four different geographical regions: (a) Northern Hemisphere land (b) North Atlantic, (c) northern stratocumulus region, and (d) tropical warm pool.

87% (stratocumulus) and 56% (Northern Hemisphere land) for homogeneous cloud scenes. Differences in cirrus cloud identification appear mostly in partly cloudy fields or multilayer clouds (see also paper 3). Confusion between midlevel and low-level clouds can be explained by discrepancies in atmospheric temperature profiles. Dust storms in desert regions may also lead to a different cloud interpretation.

Acknowledgments. The 3I processing has been performed on the computers of the Institut du Développement et des Ressources en Informatique Scientifique of the Centre National de la Recherche Scientifique. Special thanks to Alison Walker at GISS, who gave invaluable advice in the treatment of the ISCCP dataset. We also want to thank the reviewers for their helpful comments.

REFERENCES

Armante, R., L. Crépeau, N. A. Scott, and A. Chédin, 1998: Correction for spurious trends in the 3I reanalysis of TOVS data. Preprints, *Ninth Conf. on Satellite Meteorology and Oceanography*, Paris, France, Amer. Meteor. Soc., 718–720.

Cairns, B., 1995: Diurnal variations of cloud from ISCCP data. *Atmos. Res.*, **37,** 133–146.

Chédin, A., N. A. Scott, C. Wahiche, and P. Moulinier, 1985: The improved initialized inversion method: A high resolution physical method for temperature retrievals from the *TIROS-N* series. *J. Climate Appl. Meteor.*, **24,** 124–143.

——, ——, J. P. Chaboureau, F. Chéruy, C. J. Stubenrauch, R. Armante, and D. Kasysavanh, 1997: Reanalysis of a multi-year archive of TOVS NOAA satellite data for climate studies. *First Int. Conf. on the Reanalyses*, Washington, DC, NOAA, 6 pp.

Chevallier, F., F. Chéruy, N. A. Scott, and A. Chédin, 1998: A neural network approach for a fast and accurate computation of a longwave radiative budget. *J. Appl. Meteor.*, **37,** 1385–1397.

Coackley, J. A., Jr., and F. P. Bretherton, 1982: Cloud cover from high-resolution scanner data: Detecting and allowing for partially filled fields of view. *J. Geophys. Res.*, **87,** 4917–4932.

Derrien, M., B. Farki, L. Harang, H. Le Gléau, A. Noyalet, D. Pochic, and A. Sairouni, 1993: Automatic cloud detection applied to NOAA-II AVHRR imagery. *Remote Sens. Environ.*, **46,** 246–267.

Escobar, J., 1993: Base de données pour restitution de paramètres atmosphériques à l'échelle globale. Etude sur l'inversion par réseaux de neurones de données des sondeurs verticaux atmosphériques, satellitaires présents et à venir. Ph.D. dissertation, Université Pierre et Marie Curie, 167 pp. [Available from LMD, Ecole Polytechnique, 91128 Palaiseau Cédex, France.]

Eyre, J. R., and W. P. Menzel, 1989: Retrieval of cloud parameters from satellite sounder data: A simulation study. *J. Appl. Meteor.*, **28,** 267–275.

Fu, R., A. D. Del Genio, and W. B. Rossow, 1990: Behavior of deep convective clouds in the tropical Pacific deduced from ISCCP radiances. *J. Climate*, **3,** 1129–1152.

Jin, Y., and W. B. Rossow, 1997: Detection of cirrus overlapping low-level clouds. *J. Geophys. Res.*, **102,** 1727–1737.

——, ——, and D. P. Wylie, 1996: Comparison of the climatologies of high-level clouds from HIRS and ISCCP. *J. Climate.*, **9,** 2850–2879.

Kidwll, K. B., 1995: NOAA polar orbiter data users guide (*TIROS-N, NOAA-6, NOAA-7, NOAA-8, NOAA-9, NOAA-10, NOAA-11, NOAA-12, NOAA-13* and *NOAA-14*). National Oceanic and Atmospheric Administration, National Environment Satellite, Data and Information Service, Washington, DC, 394 pp.

Klein, S. A., and D. L. Hartmann, 1993: The seasonal cycle of low stratiform clouds. *J. Climate*, **6,** 1587–1606.

Lau, N.-Ch., and M. W. Crane, 1995: A satellite view of the synoptic-scale organization of cloud properties in midlatitude and tropical circulation systems. *Mon. Wea. Rev.*, **123,** 1984–2006.

Liao, X., W. B. Rossow, and D. Rind, 1995: Comparison between SAGE II and ISCCP high-level clouds. Part II: Locating cloud tops. *J. Geophys. Res.*, **100,** 1137–1147.

Lin, B., and W. B. Rossow, 1994: Observations of cloud liquid water path over oceans: Optical and microwave remote sensing methods. *J. Geophys. Res.*, **99,** 20 907–20 927.

Machado, L. A. T., and W. B. Rossow, 1993: Structural characteristics and radiative properties of tropical cloud clusters. *Mon. Wea. Rev.*, **121,** 3234–3260.

Maiden, M., G. Ohring, and J. Dodge, 1994: NOAA-NASA pathfinder program. NOAA Award NA27GP0232-01, UCAR, 22 pp. [Available from Goddard Space Flight Center, Greenbelt, MD 20771.]

McMillin, L. M., and C. Dean, 1982: Evaluation of a new operational technique for producing clear radiances. *J. Appl. Meteor.*, **21,** 1005–1014.

Menzel, W. P., D. P. Wylie, and K. I. Strabala, 1992: Seasonal and diurnal changes in cirrus clouds as seen in four years of observations with the VAS. *J. Appl. Meteor.*, **31,** 370–385.

Mishchenko, M. I., W. B. Rossow, A. Macke, and A. A. Lacis, 1996: Sensitivity of cirrus cloud albedo, bi-directional reflectance and optical thickness retrieval accuracy to ice particle shape. *J. Geophys. Res.*, **101,** 16 973–16 985.

Rossow, W. B., and R. A. Schiffer, 1991: ISCCP cloud data products. *Bull. Amer. Meteor. Soc.*, **72,** 1–20.

——, and L. C. Garder, 1993a: Cloud detection using satellite measurements of infrared and visible radiances for ISCCP. *J. Climate*, **6,** 2341–2369.

——, and ——, 1993b: Validation of ISCCP cloud detections. *J. Climate*, **6,** 2370–2393.

——, and B. Cairns, 1995: Monitoring changes of clouds. *Climate Change*, **31,** 305–347.

——, A. W. Walker, and L. C. Garder, 1993: Comparison of ISCCP and other cloud amounts. *J. Climate*, **6,** 2394–2418.

——, ——, D. Beuschel, and M. Roiter, 1996: International Satellite Cloud Climatology Project (ISCCP): Description of new cloud datasets. WMO/TD-737, World Climate Research Programme (ICSU and WMO), Geneva, Switzerland, 115 pp.

Scott, N. A., and A. Chédin, 1981: A fast line-by-line method for atmospheric absorption computations: The Automized Atmospheric Absorption Atlas. *J. Appl. Meteor.*, **20,** 802–812.

Sèze, G., and W. B. Rossow, 1991: Effects of satellite data resolution on measuring the space/time variations of surfaces and clouds. *Int. J. Remote Sens.*, **12,** 921–952.

Shea, D. J., K. E. Trenberth, and R. W. Reynolds, 1990: A global monthly sea surface temperature climatology. NCAR Tech. Note TN-345+STR, 167 pp.

Stubenrauch, C. J., N. A. Scott, and A. Chédin, 1996: Cloud field identification for earth radiation budget studies. Part I: Cloud field classification using HIRS–MSU sounder measurements. *J. Appl. Meteor.*, **35,** 416–427.

——, A. Chédin, R. Armante, and N. A. Scott, 1999a: Clouds as seen by satellite sounders (3I) and imagers (ISCCP). Part II: A new approach for cloud parameter determination in the 3I algorithms. *J. Climate*, **12,** 2214–2223.

——, W. B. Rossow, N. A. Scott, and A. Chédin, 1999b: Clouds as seen by satellite sounders (3I) and imagers (ISCCP). Part III: Spatial heteorogeneity and radiative effects. *J. Climate*, in press.

Susskind, J., P. Piraino, L. Rokke, L. Iredell, and A. Mehta, 1997: Characteristics of the TOVS pathfinder path A dataset. *Bull. Amer. Meteor. Soc.*, **78,** 1449–1472.

Tselioudis, G., W. B. Rossow, and D. Rind, 1992: Global patterns of

cloud optical thickness variation with temperature. *J. Climate,* **5,** 1484–1495.

Wahiche, C. N., N. A. Scott, and A. Chédin, 1986: Cloud detection and cloud parameter retrieval from the satellites of the *TIROS-N* series. *Ann. Geophys.,* **4B,** 207–222.

Warren, S. G., C. J. Hahn, J. London, R. M. Chervin, and R. L. Jenne, 1986: Global distribution of total cloud cover and cloud type amounts over land. NCAR Tech. Note NCAR/TN-273+STR, Boulder, CO, 29 pp. + 200 maps.

Wielicki, B. A., and L. Parker, 1992: On the determination of cloud cover from satellite sensors: The effect of sensor spatial resolution. *J. Geophys. Res.,* **97,** 12 799–12 823.

Wylie, D. P., and W. P. Menzel, 1999: Eight years of high cloud statistics using HIRS. *J. Climate,* **12,** 170–184.